CO_2 Removal by Single and Mixed Amines in a Hollow-Fiber Membrane Module—Investigation of Contactor Performance

Ion Iliuta, Francis Bougie, and Maria C. Iliuta
Dept. of Chemical Engineering, Laval University, Québec, Canada G1V 0A6

DOI 10.1002/aic.14678
Published online November 21, 2014 in Wiley Online Library (wileyonlinelibrary.com)

This work investigates CO_2 removal by single and blended amines in a hollow-fiber membrane contactor (HFMC) under gas-filled and partially liquid-filled membrane pores conditions via a two-scale, nonisothermal, steady-state model accounting for CO_2 diffusion in gas-filled pores, CO_2 and amines diffusion/reaction within liquid-filled pores and CO_2 and amines diffusion/reaction in liquid boundary layer. Model predictions were compared with CO_2 absorption data under various experimental conditions. The model was used to analyze the effects of liquid and gas velocity, CO_2 partial pressure, single (primary, secondary, tertiary, and sterically hindered alkanolamines) and mixed amines solution type, membrane wetting, and cocurrent/countercurrent flow orientation on the HFMC performance. An insignificant difference between the absorption in cocurrent and countercurrent flow was observed in this study. The membrane wetting decreases significantly the performance of hollow-fiber membrane module. *The nonisothermal simulations reveal that the* hollow-fiber membrane module *operation can be considered as nearly isothermal.* © 2014 American Institute of Chemical Engineers *AIChE J*, 61: 955–971, 2015

Keywords: CO_2 absorption, membrane partial wetting, hollow-fiber membrane contactor, experimental, modeling

Introduction

Global warming is an increasingly worrying issue for the international community. The rise of atmospheric temperature is likely correlated with the increase of anthropogenic greenhouse gas emissions. Carbon dioxide is the largest contributor to the greenhouse effect; according to the most recent Intergovernmental Panel on Climate Change report,[1] the share of CO_2 emission was 76% in 2010, while CH_4 contributed to 16%, N_2O to about 6% and the combined fluorinated gases to about 2%. The major sources of CO_2 emissions are the combustion of fossil fuels and natural gas. In addition, various industrial processes as oil refineries, cement, steel, and aluminum production annually emit huge amounts of CO_2 into the atmosphere. In this context, CO_2 capture has recently attracted a considerable interest in the reduction of industrial CO_2 emissions, aiming to separate CO_2 from different gaseous mixtures to produce a concentrated stream ready for sequestration or further use.

A large variety of CO_2 capture techniques have been proposed including absorption, adsorption, cryogenic distillation, and membrane techniques.[2–5] Among them, the absorption processes is the most extensively used technology to capture CO_2 in conventional gas–liquid contactors due to its highest CO_2 removal efficiency (up to 90%).[5] Absorption–desorption processes in which CO_2 is contacted with aqueous amine solutions such as monoethanolamine (MEA), diethanolamine (DEA), di-2-propanolamine (DIPA), and 2-amino-2-methyl-1-propanol (AMP) are the most developed schemes being used extensively in natural gas purification.[6,7] However, even if the reaction between CO_2 and these amines is significantly fast, their potential application in CO_2 capture encounters several drawbacks, the most important being the high regeneration energy requirement.[7–9] Equilibrium limitations, equipment corrosion, and amine degradation are some other drawbacks of the process, mainly inherited by the aqueous moiety.[10–15] The use of blended alkanolamine solutions has recently become very attractive because of the combination of each amine advantages: the fast reactivity of primary or secondary alkanolamines (MEA, DEA) coupled with the high absorption capacity and low solvent regeneration cost of tertiary (*N*-methyldiethanolamine—MDEA) or sterically hindered alkanolamines (SHA; AMP). In blended amines solutions, piperazine (Pz) can also be used as activator; Pz is not an alkanolamine but has proven to have a higher absorption rate than MEA.[16–21]

CO_2 capture by chemical absorption and desorption of CO_2 in aqueous amine solutions is projected to consume up to 30% of the net power generation of a coal burning power plant, causing significant economic burdens as well as an increase of the need for petroleum-based amine chemicals. Additionally, the conventional CO_2 absorption equipment (packed and tray towers, bubble columns, venture scrubbers, and spray towers) suffer from several disadvantages such as large space occupancy, high capital cost, high tendency for corrosion, and a variety of operational problems including liquid channeling, foaming, flooding, and entrainment.[22–24] To overcome the aforementioned problems, alternative technologies that can decrease the cost of CO_2 capture and minimize environmental impacts are needed. Gas–liquid

Correspondence concerning this article should be addressed to M. C. Iliuta at maria-cornelia.iliuta@gch.ulaval.ca.

membrane contactors have been proposed as a promising alternative.[25,26] Hollow-fiber membrane contactors (HFMCs) involve the transfer of CO_2 through a nonselective porous membrane, followed by its absorption into a liquid absorbent. This technology is integrated to exploit the benefits of both absorption (high selectivity) and membrane separation (modularity and compact structure)[27] and offers several advantages such as: operational flexibility, independent control of gas and liquid flow rates, high mass transfer rates, large gas/liquid interfaces with known area, compact size, easy scale-up or scale-down, and modularity.[28] The operational problems encountered in the conventional equipment are avoided because the gas stream flows on one side and the absorbent liquid flows on the other side of the membrane, without phase dispersion. However, a disadvantage of the membrane contactors is the presence of an additional diffusional resistance (through the membrane pores), which becomes significant when the membrane pores are wetted by liquid absorbents,[26,29] thus, leading to the deterioration of CO_2 absorption flux in long-term operation. Kreulen et al.[30] were the first to suggest that the wetting of membrane pores significantly impacts mass transfer coefficients in the membrane module, leading to a sharp increase in membrane resistance, and a rapid decline of the absorption performance.

Numerous investigators in the past have studied the absorption of CO_2 in different single and blended alkanolamine solvents using conventional gas–liquid contactors. The use of HFMCs started attracting the attention in the last two decades only and many experimental and theoretical studies are continuously reported to better evaluate the applicability, the performances and the limitations of this technology. Bhaumik et al.[31] developed a rapid pressure swing absorption process by integrating the best features of membrane contacting, gas–liquid absorption, and pressure swing adsorption for CO_2 cyclic separation in a microporous hydrophobic hollow-fiber module. Wang et al.[32] theoretically studied the absorption of CO_2 in HFMCs using three typical alkanolamines solutions of DEA, MDEA, and AMP. Their simulations indicated that DEA and AMP gave much higher CO_2 absorption fluxes compared to MDEA solutions. The performance of a laboratory-scale membrane contactor was investigated by Hoff et al.[33] for the case of CO_2 absorption into separate aqueous solutions of MEA and MDEA at different values of CO_2 partial pressure, liquid CO_2 loading, liquid velocity, and temperature. Zhang et al.[34] studied CO_2 absorption in aqueous DEA solutions in a HFMC at different CO_2 partial pressures. Gong et al.[35] have reported an experimental and theoretical analysis about CO_2 removal in aqueous blends of MDEA and MEA in a hollow-fiber membrane module. Their results indicated that the fractional removal of CO_2 and the CO_2 absorptions flux increased with the increase of MEA concentration in the blend. Paul et al.[36] studied the removal of CO_2 by single (MEA, DEA, MDEA, and AMP) and blended (MEA-MDEA, DEA-MDEA, MEA + AMP) aqueous alkanolamine solutions in HFMCs. The aqueous solution of MEA had the highest CO_2 absorption flux among the single amine solutions and for the absorption in mixed amines, the absorption flux increased with the increase of the concentration of MEA or DEA. Delgado et al.[37] investigated the effect of several operational variables (liquid velocity, fiber length, lean CO_2 loading, and amine concentration) on the absorption process in the case of absorption of CO_2 into aqueous DEA solutions using HFMCs. Khaisri et al.[38] studied the absorption of CO_2 in MEA solutions in a polytetrafluoroethylene (PTFE) hollow-fiber membrane module and compared the experimental data with a homogeneous mathematical model. The membrane mass transfer resistance was determined using the Wilson plot method and a theoretical approach. Partial membrane wetting was investigated to determine the effect of membrane mass transfer resistance on the absorption performance and the overall mass transfer coefficient. The maximum acceptable percent of membrane wetting in gas absorption membrane systems was found to be 40%. Rode et al.[39] evaluated the intensification potential of membrane contactors for CO_2 absorption in MEA under industrially relevant operating conditions using a generic 1-D methodology. The influence of the external fiber radius, and membrane permeability and thickness on overall process performance was investigated. Boucif et al.[40] have reported a parametric investigation of CO_2 absorption in MEA by a HFMC using a model based on the momentum and mass transport conservation laws in all three compartments. In the shell side, the flow was described by the Navier–Stokes momentum balance equations. Ghasem et al.[41] studied the effect of water evaporation on the performance of CO_2 absorption in HFMCs using aqueous sodium hydroxide solutions. Zaidiza et al.[42] compared 1-D and 2-D modeling approaches of CO_2 postcombustion capture process in HFMCs and concluded that 1-D model provided similar results with 2-D model in the investigated domain, with significant lower calculation times. Also, Chabanon et al.[43] have reported a critical comparative analysis of modeling strategies for CO_2 capture by absorption in MEA solutions. Four different types of models (constant overall mass transfer coefficient model, 1-D resistance in series, 1-D and 2-D convection–diffusion models) have been compared, with the membrane mass transfer coefficient as the only adjustable parameter. It was shown that the different models performed equally well in terms of fit efficiency, whatever their intrinsic level of complexity, when similar membrane mass transfer coefficient values were used. This result addresses key questions in terms of strategy for model validation and with regard to the current trend of increasing model complexity.

Although the advancements accomplished up till now in the modeling of CO_2 absorption process in gas–liquid membrane contactors are noticeable, none of the available approaches attempted, to the best of our knowledge, to harness into a comprehensive model the following phenomena: (1) CO_2 diffusion in the gas-filled membrane pores, CO_2 and amines diffusion/reaction within the liquid-filled membrane pores, (2) CO_2 and amines diffusion/reaction in the liquid boundary layer, (3) mass and momentum balance equations in the bulk liquid and gas phases, (4) variable gas flow rate due to chemical contraction, and (5) thermal effects, heat transfer, and interfacial temperatures using properly formulated enthalpy balance equations.

This work is offered as an incremental piece of information in this direction and proposes the investigation of CO_2 absorption accompanied by chemical reaction with single and mixed amines in hollow-fiber membrane absorbers under gas-filled pores and partially liquid-filled pores conditions using a new two-scale, nonisothermal, steady-state model harnessing the five aforementioned features. We first summarize the main steps for developing the model accounting for CO_2 diffusion in the gas-filled membrane pores, CO_2 and amines diffusion/reaction within the liquid-filled membrane pores and, CO_2 and amines diffusion/reaction in the liquid boundary layer. The liquid film zone surrounding the inside

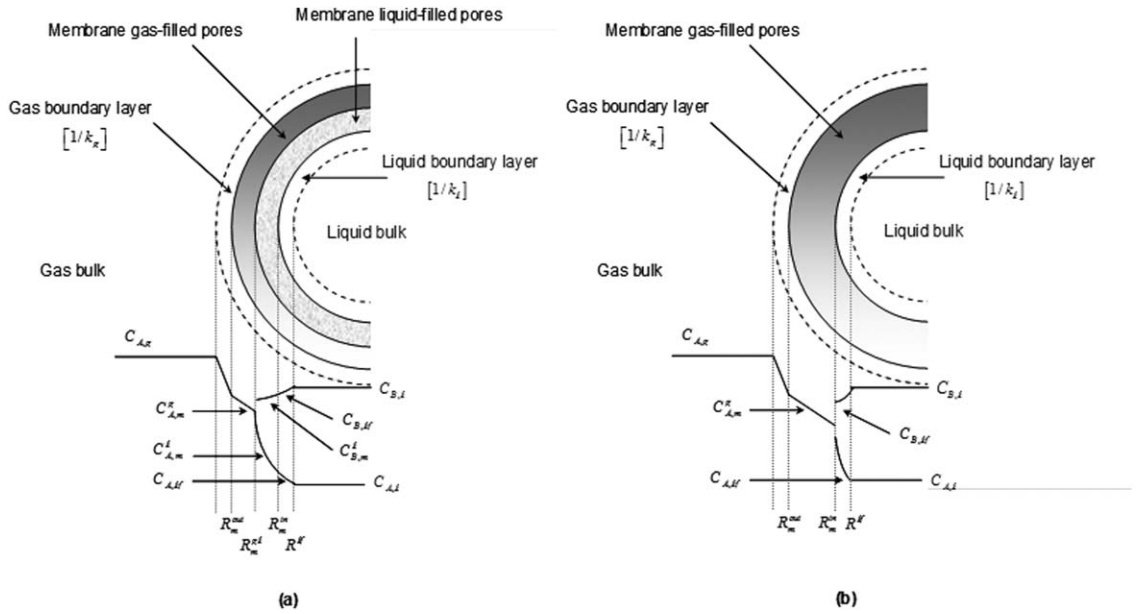

Figure 1. Schematic diagram of absorption process in hollow-fiber membrane: (a) membrane partially liquid-filled pores; (b) membrane gas-filled pores.

membrane wall was described by the nonlinear differential equations governing diffusion and reaction given by the film theory and the bulk liquid phase within the hollow-fiber was modeled assuming "concentration plug flow" under laminar flow conditions.[44,45] In the second part of the work, we propose to analyze the simulated effects of the liquid and gas velocity, CO_2 partial pressure, single and mixed amine solution type, and membrane wetting on the membrane module performance. The impact of the cocurrent and countercurrent flow orientation was investigated. CO_2 removal by single primary (MEA), secondary (DEA), tertiary (MDEA), and SHA (AMP, a simple hindrance form of MEA and three SHA derived from AMP: 2-amino-2-methyl-1,3-propanediol (AMPD), 2-amino-2-ethyl-1,3-propanediol (AEPD), and 2-amino-2-hydroxymethyl-1,3-propanediol (AHPD)), and mixed amines (MEA-MDEA, MEA-AMP, AHPD-Pz) was considered in the study. The model predictions were compared with CO_2 absorption data obtained in a HFMC under various experimental conditions.

Theoretical Background

When the membrane pores are partially filled with liquid absorbent (real operating conditions), the two-scale, nonisothermal, steady-state model of the gas–liquid hollow-fiber membrane module describes CO_2 diffusion in the gas-filled membrane pores and the diffusion accompanied by the chemical reaction of CO_2 and amines within the liquid-filled membrane pores (Figure 1a). Under membrane gas-filled pores conditions, the mathematical model describe only the mass transfer of CO_2 through the membrane pores, followed by its absorption into the liquid absorbent (Figure 1b). The liquid film zone surrounding the inside membrane wall is described by the nonlinear differential equations governing diffusion and reaction of CO_2 and amines, given by the film theory developed by Lewis and Whitman[46] (Henry's law holds). The model equations at the gas–liquid membrane contactor level consist of mass balance equations for both gas and liquid phases under nonisothermal conditions. Bulk liquid phase within the fiber lumen was modeled assuming "concentration plug flow" under laminar flow conditions.

Reaction mechanism in aqueous amine solutions

The kinetics of the reaction between CO_2 and aqueous amines were described via the mechanism proposed by Caplow[47] and redeveloped by Danckwerts[48] which assumes the formation of a zwitterion followed by the removal of a proton by all bases existing in solution. This mechanism has been used successfully with conventional alkanolamines and SHA, such as MEA, DEA, DIPA, AHPD, AEPD, and AMPD[21,49–51]

$$\mathrm{RNH_2} + \mathrm{CO_2} \underset{k_{-1}}{\overset{k_2}{\rightleftarrows}} \mathrm{RNH_2^+COO^-} \tag{1}$$

$$\mathrm{RNH_2^+COO^-} + \mathrm{Base} \underset{k_{-b}}{\overset{k_b}{\rightleftarrows}} \mathrm{RNHCOO^-} + \mathrm{BaseH^+} \tag{2}$$

For this mechanism, the overall forward reaction rate equation, derived with the assumption of quasi-steady-state condition for the zwitterion concentration and irreversible deprotonation of the zwitterion by bases, is

$$r_{\mathrm{CO_2-RNH_2}} = \frac{k_2[\mathrm{CO_2}][\mathrm{RNH_2}]}{1 + \frac{k_{-1}}{\sum k_b[\mathrm{Base}]}} \tag{3}$$

where $\sum k_b[\mathrm{Base}]$ is the contribution to the removal of the proton by all bases present in the solution.

For the reaction between CO_2 and tertiary amines (MDEA) and Pz a second-order reaction rate was used[11,20,36,52]

$$r_{\mathrm{CO_2-Am}} = k_2[\mathrm{CO_2}][\mathrm{Am}] \tag{4}$$

Porous membrane scale model

In real conditions, the membrane pores are partially filled with the liquid absorbent. Consequently, the mathematical model at the porous membrane level describes the diffusion

of carbon dioxide in the dried membrane layer and the diffusion accompanied by the chemical reaction of carbon dioxide within the wetted membrane layer. In addition, the model contains the steady-state mass balance equations which describe the amines diffusion accompanied by chemical reaction within the wetted membrane layer.

Steady-state mass balance equations which describe CO_2 (A) diffusion within the membrane gas-filled pores and CO_2 diffusion accompanied by the chemical reaction within the membrane liquid-filled pores[53] are

$$D_{\mathrm{A,g}}^{\mathrm{eff}}\left[\frac{1}{r}\frac{\partial}{\partial r}\left(r\frac{\partial C_{\mathrm{A,m}}^{\mathrm{g}}}{\partial r}\right)\right]=0 \tag{5}$$

$$D_{\mathrm{A,l}}^{\mathrm{eff}}\left[\frac{1}{r}\frac{\partial}{\partial r}\left(r\frac{\partial C_{\mathrm{A,m}}^{\mathrm{l}}}{\partial r}\right)\right]-\sum_{i=1}^{2}v_{\mathrm{A},i}r_i\left(C_{j,\mathrm{m}}^{\mathrm{l}}\right)=0 \tag{6}$$

The corresponding boundary conditions are given as (gas–liquid interface is positioned in membrane)

$$r=R_{\mathrm{m}}^{\mathrm{out}}\qquad k_{\mathrm{g}}\left(C_{\mathrm{A,g}}-C_{\mathrm{A,m}}^{\mathrm{g}}\big|_{r=R_{\mathrm{m}}^{\mathrm{out}}}\right)=-D_{\mathrm{A,g}}^{\mathrm{eff}}\frac{\partial C_{\mathrm{A,m}}^{\mathrm{g}}}{\partial r}\bigg|_{r=R_{\mathrm{m}}^{\mathrm{out}}} \tag{7}$$

$$r=R_{\mathrm{m}}^{\mathrm{gl}}\qquad D_{\mathrm{A,g}}^{\mathrm{eff}}\frac{\partial C_{\mathrm{A,m}}^{\mathrm{g}}}{\partial r}\bigg|_{r=R_{\mathrm{m}}^{\mathrm{gl}}}=D_{\mathrm{A,l}}^{\mathrm{eff}}\frac{\partial C_{\mathrm{A,m}}^{\mathrm{l}}}{\partial r}\bigg|_{r=R_{\mathrm{m}}^{\mathrm{gl}}} \tag{8}$$

$$C_{\mathrm{A,m}}^{\mathrm{g}}\big|_{r=R_{\mathrm{m}}^{\mathrm{gl}}}=C_{\mathrm{A,m}}^{\mathrm{l}}\big|_{r=R_{\mathrm{m}}^{\mathrm{gl}}}\frac{1}{m} \tag{9}$$

$$r=R_{\mathrm{m}}^{\mathrm{in}}\qquad D_{\mathrm{A,l}}^{\mathrm{eff}}\frac{\partial C_{\mathrm{A,m}}^{\mathrm{l}}}{\partial r}\bigg|_{r=R_{\mathrm{m}}^{\mathrm{in}}}=D_{\mathrm{A,l}}\frac{\partial C_{\mathrm{A,lf}}}{\partial r}\bigg|_{r=R_{\mathrm{m}}^{\mathrm{in}}} \tag{10}$$

The steady-state mass balance equation which describe amines (j = B, C) diffusion accompanied by the chemical reaction within the membrane liquid-filled pores is

$$D_{j,\mathrm{l}}^{\mathrm{eff}}\left[\frac{1}{r}\frac{\partial}{\partial r}\left(r\frac{\partial C_{j,\mathrm{m}}^{\mathrm{l}}}{\partial r}\right)\right]-R_j=0 \tag{11}$$

The corresponding boundary conditions are based on the following assumptions: the component j is nonvolatile and at the membrane–liquid interface the flux of component j in the liquid film is equal to the flux in the wetted part of the membrane

$$r=R_{\mathrm{m}}^{\mathrm{gl}}\qquad D_{j,\mathrm{l}}^{\mathrm{eff}}\frac{\partial C_{j,\mathrm{m}}^{\mathrm{l}}}{\partial r}\bigg|_{r=R_{\mathrm{m}}^{\mathrm{gl}}}=0 \tag{12}$$

$$r=R_{\mathrm{m}}^{\mathrm{in}}\qquad D_{\mathrm{j,l}}^{\mathrm{eff}}\frac{\partial C_{j,\mathrm{m}}^{\mathrm{l}}}{\partial r}\bigg|_{r=R_{\mathrm{m}}^{\mathrm{in}}}=D_{j,\mathrm{l}}\frac{\partial C_{j,\mathrm{lf}}}{\partial r}\bigg|_{r=R_{\mathrm{m}}^{\mathrm{in}}} \tag{13}$$

Under nonisothermal conditions, the temperature gradients in the membrane pores are given by the equations describing the heat transport within the membrane gas-filled pores and the heat transport and reaction within the membrane liquid-filled pores (convective terms are assumed to be insignificant)[53]

$$\lambda_{\mathrm{m,g}}^{\mathrm{eff}}\left[\frac{1}{r}\frac{\partial}{\partial r}\left(r\frac{\partial T_{\mathrm{m}}^{\mathrm{g}}}{\partial r}\right)\right]=0 \tag{14}$$

$$\lambda_{\mathrm{m,l}}^{\mathrm{eff}}\left[\frac{1}{r}\frac{\partial}{\partial r}\left(r\frac{\partial T_{\mathrm{m}}^{\mathrm{l}}}{\partial r}\right)\right]+\sum_{i=1}^{2}r_i\left(C_{j,\mathrm{m}}^{\mathrm{l}}\right)(-\Delta H_{Ri})=0 \tag{15}$$

$$r=R_{\mathrm{m}}^{\mathrm{out}}\qquad \alpha_{\mathrm{g}}\left(T_{\mathrm{g}}-T_{\mathrm{m}}^{\mathrm{g}}\big|_{r=R_{\mathrm{m}}^{\mathrm{out}}}\right)=-\lambda_{\mathrm{m,g}}^{\mathrm{eff}}\frac{\partial T_{\mathrm{m}}^{\mathrm{g}}}{\partial r}\bigg|_{r=R_{\mathrm{m}}^{\mathrm{out}}} \tag{16}$$

$$r=R_{\mathrm{m}}^{\mathrm{gl}}\qquad \lambda_{\mathrm{m,g}}^{\mathrm{eff}}\frac{\partial T_{\mathrm{m}}^{\mathrm{g}}}{\partial r}\bigg|_{r=R_{\mathrm{m}}^{\mathrm{gl}}}=\lambda_{\mathrm{m,l}}^{\mathrm{eff}}\frac{\partial T_{\mathrm{m}}^{\mathrm{l}}}{\partial r}\bigg|_{r=R_{\mathrm{m}}^{\mathrm{gl}}} \tag{17}$$

$$T_{\mathrm{m}}^{\mathrm{g}}\big|_{r=R_{\mathrm{m}}^{\mathrm{gl}}}=T_{\mathrm{m}}^{\mathrm{l}}\big|_{r=R_{\mathrm{m}}^{\mathrm{gl}}} \tag{18}$$

$$r=R_{\mathrm{m}}^{\mathrm{in}}\qquad \lambda_{\mathrm{m,l}}^{\mathrm{eff}}\frac{\partial T_{\mathrm{m}}^{\mathrm{l}}}{\partial r}\bigg|_{r=R_{\mathrm{m}}^{\mathrm{in}}}=\lambda_{\mathrm{l}}\frac{\partial T_{\mathrm{lf}}}{\partial r}\bigg|_{r=R_{\mathrm{m}}^{\mathrm{in}}} \tag{19}$$

Under membrane gas-filled pores (ideal) conditions the mathematical model describe only the mass transfer of CO_2 and heat transport through the membrane pores and is reduced to the Eqs. 5 and 14 with the following boundary conditions

$$r=R_{\mathrm{m}}^{\mathrm{out}}\qquad k_{\mathrm{g}}\left(C_{\mathrm{A,g}}-C_{\mathrm{A,m}}^{\mathrm{g}}\big|_{r=R_{\mathrm{m}}^{\mathrm{out}}}\right)=-D_{\mathrm{A,g}}^{\mathrm{eff}}\frac{\partial C_{\mathrm{A,m}}^{\mathrm{g}}}{\partial r}\bigg|_{r=R_{\mathrm{m}}^{\mathrm{out}}} \tag{20}$$

$$\alpha_{\mathrm{g}}\left(T_{\mathrm{g}}-T_{\mathrm{m}}^{\mathrm{g}}\big|_{r=R_{\mathrm{m}}^{\mathrm{out}}}\right)=-\lambda_{\mathrm{m,g}}^{eff}\frac{\partial T_{\mathrm{m}}^{\mathrm{g}}}{\partial r}\bigg|_{r=R_{\mathrm{m}}^{\mathrm{out}}} \tag{21}$$

$$r=R_{\mathrm{m}}^{\mathrm{in}}\qquad D_{\mathrm{A,g}}^{\mathrm{eff}}\frac{\partial C_{\mathrm{A,m}}^{\mathrm{g}}}{\partial r}\bigg|_{r=R_{\mathrm{m}}^{\mathrm{in}}}=D_{\mathrm{A,l}}\frac{\partial C_{\mathrm{A,lf}}}{\partial r}\bigg|_{r=R_{\mathrm{m}}^{\mathrm{in}}} \tag{22}$$

$$\lambda_{\mathrm{m,g}}^{\mathrm{eff}}\frac{\partial T_{\mathrm{m}}^{\mathrm{g}}}{\partial r}\bigg|_{r=R_{\mathrm{m}}^{\mathrm{in}}}=\lambda_{\mathrm{l}}\frac{\partial T_{\mathrm{lf}}}{\partial r}\bigg|_{r=R_{\mathrm{m}}^{\mathrm{in}}} \tag{23}$$

Liquid boundary layer (liquid film) scale model

In the liquid phase, the reaction zone is located near the inside membrane wall where the liquid motion by convection is slight compared to that in the main body of liquid and a stationary liquid film can be considered. So, the small liquid zone surrounding the inside membrane wall can be described by a system of nonlinear differential equations governing diffusion and reaction of CO_2 and amines, given by the film theory developed by Lewis and Whitman[46]

$$D_{\mathrm{A,l}}\left[\frac{1}{r}\frac{\partial}{\partial r}\left(r\frac{\partial C_{\mathrm{A,lf}}}{\partial r}\right)\right]-\sum_{i=1}^{2}v_{\mathrm{A},i}r_i\left(C_{j,\mathrm{lf}}\right)=0 \tag{24}$$

$$D_{j,\mathrm{l}}\left[\frac{1}{r}\frac{\partial}{\partial r}\left(r\frac{\partial C_{j,\mathrm{lf}}}{\partial r}\right)\right]-R_j\left(C_{j,\mathrm{lf}}\right)=0\quad\text{where } j=\mathrm{B,C} \tag{25}$$

Under nonisothermal conditions, the temperature gradient in the liquid film is given by the following heat transport equation[53]

$$\lambda_{\mathrm{l}}\left[\frac{1}{r}\frac{\partial}{\partial r}\left(r\frac{\partial T_{\mathrm{lf}}}{\partial r}\right)\right]+\sum_{i=1}^{2}r_i\left(C_{j,\mathrm{lf}}\right)(-\Delta H_{Ri})=0 \tag{26}$$

When the membrane pores are partially filled with liquid, the boundary conditions are as follows

$$r=R_{\mathrm{m}}^{\mathrm{in}}\quad D_{j,\mathrm{l}}^{\mathrm{eff}}\frac{\partial C_{j,\mathrm{m}}^{\mathrm{l}}}{\partial r}\bigg|_{r=R_{\mathrm{m}}^{\mathrm{in}}}=D_{j,\mathrm{l}}\frac{\partial C_{j,\mathrm{lf}}}{\partial r}\bigg|_{r=R_{\mathrm{m}}^{\mathrm{in}}}\quad\text{where } j=\mathrm{A,\ B,\ C} \tag{27}$$

$$\lambda_{\mathrm{m,l}}^{\mathrm{eff}}\frac{\partial T_{\mathrm{m}}^{\mathrm{l}}}{\partial r}\bigg|_{r=R_{\mathrm{m}}^{\mathrm{in}}}=\lambda_{\mathrm{l}}\frac{\partial T_{\mathrm{lf}}}{\partial r}\bigg|_{r=R_{\mathrm{m}}^{\mathrm{in}}} \tag{28}$$

$$r=R^{\mathrm{lf}}\quad C_{j,\mathrm{lf}}|_{r=R^{\mathrm{lf}}}=C_{j,\mathrm{l}}\quad \text{where } j=\mathrm{A},\ \mathrm{B},\ \mathrm{C} \tag{29}$$

$$T_{\mathrm{lf}}|_{r=R^{\mathrm{lf}}}=T_{\mathrm{l}} \tag{30}$$

When the membrane pores are totally filled with gas, the boundary conditions for the liquid film model are (gas–liquid interface is positioned at membrane wall)

$$r=R_{\mathrm{m}}^{\mathrm{in}}\qquad C_{\mathrm{A,lf}}|_{r=R_{\mathrm{m}}^{\mathrm{in}}}=C_{\mathrm{A,m}}^{\mathrm{g}}|_{r=R_{\mathrm{m}}^{\mathrm{in}}}m \tag{31}$$

$$\frac{\partial C_{j,\mathrm{lf}}}{\partial r}\bigg|_{r=R_{\mathrm{m}}^{\mathrm{in}}}=0\quad \text{where } j=\mathrm{B},\ \mathrm{C} \tag{32}$$

$$\lambda_{\mathrm{m,g}}^{\mathrm{eff}}\frac{\partial T_{\mathrm{m}}^{\mathrm{g}}}{\partial r}\bigg|_{r=R_{\mathrm{m}}^{\mathrm{in}}}=\lambda_{\mathrm{l}}\frac{\partial T_{\mathrm{lf}}}{\partial r}\bigg|_{r=R_{\mathrm{m}}^{\mathrm{in}}} \tag{33}$$

$$r=R^{\mathrm{lf}}\quad C_{j,\mathrm{lf}}|_{r=R^{\mathrm{lf}}}=C_{j,\mathrm{l}}\quad \text{where } j=\mathrm{A},\ \mathrm{B},\ \mathrm{C} \tag{34}$$

$$T_{\mathrm{lf}}|_{r=R^{\mathrm{lf}}}=T_{\mathrm{l}} \tag{35}$$

Gas–liquid membrane contactor scale model

The entire liquid flow in the lumen side may be viewed as consisting of three sections[54]: the so-called hydrodynamic inlet section, the concentration inlet section, and the fully developed section. In the hydrodynamic inlet section, the initially flat liquid velocity profile evolves toward a parabolic velocity profile which remains translationally invariant in the downstream direction. The hydrodynamic inlet section is estimated to be fairly short (<1 mm) compared to the total length of the hollow fiber and we may consider that the laminar flow with a parabolic velocity profile is developed from the entrance of the fiber. Due to the CO_2-amine reaction in the membrane liquid-filled pores and in the liquid film zone near the inside membrane wall, the depletion of amine as well as the saturation of the bulk liquid with CO_2 are not very important in fully established region.[44,45,55] As result, the bulk liquid flow within the hollow fiber can be modeled assuming "concentration plug flow" under laminar flow conditions.[44,45] Consequently, the steady-state mass balance equations for CO_2 and amines in the liquid phase are

$$u_{\mathrm{l}}\frac{\partial C_{\mathrm{A,l}}}{\partial z}=-D_{\mathrm{A,l}}\frac{\partial C_{\mathrm{A,lf}}}{\partial r}|_{r=R^{\mathrm{lf}}}a_{v,\mathrm{in}}-\sum_{i=1}^{2}\nu_{\mathrm{A},i}r_i\left(C_{j,\mathrm{l}}\right) \tag{36}$$

$$u_{\mathrm{l}}\frac{\partial C_{j,\mathrm{l}}}{\partial z}=-D_{j,\mathrm{l}}\frac{\partial C_{j,\mathrm{lf}}}{\partial r}\bigg|_{r=R^{\mathrm{lf}}}a_{v,\mathrm{in}}-R_j\left(C_{j,\mathrm{l}}\right)\ \text{where } j=\mathrm{B},\ \mathrm{C} \tag{37}$$

Similarly, the steady-state mass balance equation for CO_2 in the gas phase within the shell side is

$$\pm\frac{\partial\left(u_{\mathrm{g}}C_{\mathrm{A,g}}\right)}{\partial z}=D_{\mathrm{A,g}}^{\mathrm{eff}}\frac{\partial C_{\mathrm{A,m}}^{\mathrm{g}}}{\partial r}\bigg|_{r=R_{\mathrm{m}}^{\mathrm{out}}}a_{v,\mathrm{out}} \tag{38}$$

where the axial gradient of the gas velocity was obtained from the overall mass balance equation in gas phase

$$\pm\frac{\partial}{\partial z}\left(u_{\mathrm{g}}\frac{P_{\mathrm{g}}}{RT_{\mathrm{g}}}\right)=-k_{\mathrm{g}}\left(C_{\mathrm{A,g}}-C_{\mathrm{A,m}}^{\mathrm{g}}|_{r=R_{\mathrm{m}}^{\mathrm{out}}}\right)a_{v,\mathrm{out}} \tag{39}$$

Under nonisothermal conditions, the gas–liquid membrane contactor scale model is extended with the steady-state heat balance equations in the liquid and gas phases[53]

$$\rho_{\mathrm{l}}u_{\mathrm{l}}c_{\mathrm{pl}}\frac{\partial T_{\mathrm{l}}}{\partial z}=-\lambda_{\mathrm{l}}\frac{\partial T_{\mathrm{lf}}}{\partial r}\bigg|_{r=R^{\mathrm{lf}}}a_{v,\mathrm{in}}+\sum_{i=1}^{2}r_i\left(C_{j,\mathrm{l}}\right)\left(-\Delta H_{ri}\right) \tag{40}$$

$$\pm\rho_{\mathrm{g}}u_{\mathrm{g}}c_{\mathrm{pg}}\frac{\partial T_{\mathrm{g}}}{\partial z}=\lambda_{\mathrm{m,g}}^{\mathrm{eff}}\frac{\partial T_{\mathrm{m}}^{\mathrm{g}}}{\partial r}\bigg|_{r=R_{\mathrm{m}}^{\mathrm{out}}}a_{v,\mathrm{out}} \tag{41}$$

In the Eqs. 38, 39, and 41 the sign "−" corresponds to the countercurrent flow, and the sign "+"corresponds to the cocurrent flow.

For cocurrent flow, the corresponding boundary conditions are given as

$$z=0\quad C_{\mathrm{A,g}}|_{z=0}=C_{\mathrm{A,g}}^{\mathrm{in}}\quad u_{\mathrm{g}}|_{z=0}=u_{\mathrm{g}}^{\mathrm{in}} \tag{42}$$

$$C_{j,\mathrm{l}}|_{z=0}=C_{j,\mathrm{l}}^{\mathrm{in}}\quad \text{where } j=\mathrm{B},\ \mathrm{C} \tag{43}$$

$$T_{\mathrm{l}}|_{z=0}=T_{\mathrm{l}}^{\mathrm{in}}\quad T_{\mathrm{g}}|_{z=0}=T_{\mathrm{g}}^{\mathrm{in}} \tag{44}$$

For countercurrent flow, the boundary conditions are

$$z=H\quad C_{\mathrm{A,g}}|_{z=H}=C_{\mathrm{A,g}}^{\mathrm{in}}\quad u_{\mathrm{g}}|_{z=H}=u_{\mathrm{g}}^{\mathrm{in}}\quad T_{\mathrm{g}}|_{z=0}=T_{\mathrm{g}}^{\mathrm{in}} \tag{45}$$

$$z=0\quad C_{j,\mathrm{l}}|_{z=0}=C_{j,\mathrm{l}}^{\mathrm{in}}\quad T_{\mathrm{l}}|_{z=0}=T_{\mathrm{l}}^{\mathrm{in}}\quad \text{where } j=\mathrm{B},\ \mathrm{C} \tag{46}$$

Because the flow through the fibers is considered to be laminar, the internal (liquid) pressure drop was estimated using the classic Hagen–Poiseuille equation for pipe flow.[39] The pressure drop for the external (gas) flow was estimated using a Kozeny-type equation for axial flow through an array of cylinders[39] in which the Kozeny constant is fitted to a fiber-bundle geometry[56]

$$-\frac{\partial P_{\mathrm{l}}}{\partial z}=\frac{8\mu_{\mathrm{l}}}{\left(r_{\mathrm{m}}^{\mathrm{out}}-\delta\right)^2}\frac{u_{\mathrm{l}}}{\varepsilon_{\mathrm{l}}}=\frac{8\mu_{\mathrm{l}}}{\left(r_{\mathrm{m}}^{\mathrm{out}}\right)^2\left(1-\frac{\delta}{r_{\mathrm{m}}^{\mathrm{out}}}\right)^4\varphi}u_{\mathrm{l}} \tag{47}$$

$$-\frac{\partial P_{\mathrm{g}}}{\partial z}=\frac{4\kappa\mu_{\mathrm{g}}}{\left(r_{\mathrm{m}}^{\mathrm{out}}\right)^2}\frac{\varphi^2}{1-\varphi^3}u_{\mathrm{g}} \tag{48}$$

where

$$\kappa=5.5\varphi^2-7.87\varphi+7.43 \tag{49}$$

Model parameters

The effective diffusion coefficients were evaluated considering both molecular and Knudsen diffusion processes[57]

$$\frac{1}{D_j^{\mathrm{eff}}}=\frac{\tau}{\varepsilon}\left(\frac{1}{D_j}+\frac{1}{D_{kj}}\right) \tag{50}$$

The diffusion coefficients for binary gas systems were predicted with Chapman and Enskog equation[58] and the molecular gas diffusivity coefficients in multicomponent gas mixtures were calculated with Blanc correlation.[58] Knudsen diffusion coefficient was evaluated using the correlation presented in Treybal.[59] The molecular diffusion coefficients in the liquid phase was taken from Versteeg and van Swaaij[60] and Thomas and Furzer[61] or calculated using the method Wilke–Chang.[58] The solubility of CO_2 in the liquid phase was taken from Versteeg and van Swaaij,[21,60] Bougie and Iliuta,[21] Yoon et al.,[50] Yoon et al.[51] and Bishnoi and Rochelle.[11] The thermal conductivity of the amine solutions was estimated using Filippov equation and Sastri method.[62] The effective thermal conductivity of the membrane was evaluated with the porous solid model developed by Harriott[63]

Table 1. Kinetic Parameters—Single Amine Systems (at 298 K)

System	$k_{2,B}$ (m^3/kmol s)	$k_{2,B}k_{H_2O}/k_{-1}$ (m^6/kmol^{2}s)	$k_{2,B}k_B/k_{-1}$ (m^6/kmol^{2}s)	Reference
MEA(B) + H_2O	6358	9.58	1580	Liao and Li[80]
DEA(B) + H_2O	2375	2.2	437	Xu et al.[81]
AMP(B) + H_2O	810	2.64	2335	Xu et al.[81]
AMPD(B) + H_2O	301.5	1.207	298	Yoon et al.[51]
AEPD(B) + H_2O	242	0.01255	270.9	Yoon et al.[50]
AHPD(B) + H_2O	192.3	1.77	248.7	Bougie and Iliuta[21]
MDEA(B) + H_2O	5.21			Littel et al.[82]

$$\lambda_m^{eff} = \lambda_s \frac{1-\varepsilon}{\tau} \quad (51)$$

The heat capacities of amine solutions were evaluated using data from Pagé et al.[64], Chiu and Li,[65] Zhang and Chen,[66] and Olivia et al.[67,68] The reaction enthalpies were evaluated using data from Arcis et al.,[69] Gabrielsen et al.,[70] Park et al.,[71] Baek and Yoon,[72] Rodier et al.,[73] Liu et al.,[74] Mathonat et al.,[75] and Kim and Svendsen.[76] For the liquid flow in the fiber lumen, the physical liquid mass transfer coefficient was evaluated from the Graetz–Leveque correlation[77]

$$Sh_l = \frac{k_l d_m^{in}}{D_{j,l}} = 1.62\left[\frac{d_m^{in}}{H} Re_l Sc_l\right]^{1/3} \quad (52)$$

For the gas flow in the shell side, the mass transfer coefficient was evaluated with the following correlation[78]

$$Sh_g = \frac{k_g d_m^{out}}{D_{j,g}} = 0.9\, Re_g^{0.5} Sc_g^{0.33} \quad (53)$$

Heat transfer coefficient for the external flow was evaluated using Sparrow et al.[79] correlation developed for the convective heat transfer of air over a circular cylinder

$$Nu_g = \frac{\alpha_g d_m^{out}}{\lambda_g} = 0.25 + \left[0.4\, Re_g^{1/2} + 0.06\, Re_g^{2/3}\right] Pr_g^{0.37}\left(\frac{\mu_g}{\mu_w}\right)^{1/4} \quad (54)$$

The kinetic constants for all single and blended amine systems are listed in Tables 1 and 2 and the rate expressions for all amines are given in Table 3.

Numerical implementation

Aspen Custom Modeler from Aspen Tech was used to generate the numerical platform to solve the mixed ordinary differential equations (ODE)/algebraic system which models the gas–liquid HFMC. A first-order backward finite difference method was used for the discretization in the axial direction and a second-order central finite difference method in the radial direction. A nonlinear solver based on the Newton method was used to solve the set of simultaneous model equations.

Experimental

Chemicals

The aqueous amines solutions used in this work were prepared by gravimetric method. The MEA (from Sigma-Aldrich) had a minimum purity of 99% and was used without further purification. A Mettler AE240 balance with a precision of $\pm 1 \times 10^{-4}$ g was used to prepare the solutions and the uncertainties of the reported concentrations were calculated to be <0.01 wt%. Gases (CO_2 and N_2) were of commercial grade with a minimum purity of 99.9% (Praxair).

Membrane module

The membrane module used for CO_2 absorption process was fabricated from PTFE hollow-fiber membranes supplied by Markel Corporation (Pennsylvania). The hollow-fiber membranes were potted with epoxy at both ends in stainless steel discs having small holes positioned in a circular pattern. The length of the membrane inside the disc (0.03 m) on the liquid entry side gave sufficient distance ($>10d_m^{in}$) for the laminar liquid flow inside the fiber to be fully developed before it contacts the gas.[84] Additionally, the holes in the discs were sufficiently distant one relative to each other to assure evenly spaced fiber and no contact between them. This membrane assembly was put in a clear borosilicate housing allowing visual inspections of the membranes to detect any possible liquid going to the shell side through the membrane pores. Membrane and module specifications are provided in Table 4.

Absorption setup and procedure

A detailed description of the experimental setup of CO_2 absorption process can be found in Bougie et al.[85] The inlet gas flow rate and gas composition were adjusted with mass flow controllers (OMEGA, FMA-2600A) and the outlet gas flow rate and composition were determined with a bubble flowmeter and a gas chromatograph (Micro GC 3000A, Inficon). Aqueous amine solutions were supplied using a gear pump (Cole-Parmer, OF-75211) and a calibrated rotameter. Inlet and outlet fluid pressures were measured by four pressure transducers (Omega, PX481A). A needle valve at the liquid exit of the contactor was adjusted to keep the liquid-phase outlet pressure above the gas-phase pressure by at least 0.13–0.2 bar.

All experiments were performed at 298 K with the liquid flowing through the membrane lumen and the gas supplied to the shell side. The fluids were circulating countercurrently or cocurrently by modifying the gas connexions in the contactor module. Three MEA aqueous solutions were tested. The liquid flow was first established through the contactor at a rate between 10 and 80 ml/min and the liquid pressure was stabilized. A constant humidified 300 ml/min total gas flow

Table 2. Kinetic Parameters—Blended Amines System (at 298 K)

System	$k_{2,B}$ ($k_{2,C}$) (m^3/kmol s)	$k_{2,B}k_{H_2O}/k_{-1}$ ($k_{2,C}k_{H_2O}/k_{-1}$) (m^6/kmol^{2}s)	$k_{2,B}k_B/k_{-1}$ ($k_{2,C}k_C/k_{-1}$) (m^6/kmol^{2}s)	$k_{2,B}k_C/k_{-1}$ ($k_{2,C}k_B/k_{-1}$) (m^6/kmol^{2}s)	Reference
MEA(B) + MDEA(C) + H_2O	6358 (5.41)	9.58	1580	434	Liao and Li[80]
MEA(B) + AMP(C) + H_2O	5600 (560)	98 (18)	2.58×10^5 (800)	6×10^4 (9.08×10^4)	Ali[83]; Paul et al.[36]
AHPD(B) + PZ(C) + H_2O	192.3 (5.37×10^4)	1.77	248.7		Bougie et al.[20]

Table 3. Reaction Rate Expressions

Aqueous Amine Solution	r_{CO_2-B} (kmol/m^{3}s)	r_{CO_2-C} (kmol/m^{3}s)
Single amines		
MEA, DEA, AMP, AMPD, AEPD, AHPD (B)	$\frac{k_{2,B}C_AC_B}{1+\frac{1}{\left[\frac{k_{H_2O}}{k_{-1}}C_{H_2O}\right]+\left[\frac{k_B}{k_{-1}}C_B\right]}}$	
MDEA, PZ(B)	$k_{2,B}C_AC_B$	
Blended amines		
MEA(B) + MDEA(C) or AHPD(B) + PZ(C)	$\frac{k_{2,B}C_AC_B}{1+\frac{1}{\left[\frac{k_{H_2O}}{k_{-1}}C_{H_2O}\right]+\left[\frac{k_B}{k_{-1}}C_B\right]+\left[\frac{k_C}{k_{-1}}C_C\right]}}$	$k_{2,C}C_AC_C$
MEA(B) + AMP(C)	$\frac{k_{2,B}C_AC_B}{1+\frac{1}{\left[\frac{k_{H_2O}}{k_{-1}}C_{H_2O}\right]+\left[\frac{k_B}{k_{-1}}C_B\right]+\left[\frac{k_C}{k_{-1}}C_C\right]}}$	$\frac{k_{2,C}C_AC_C}{1+\frac{1}{\left[\frac{k_{H_2O}}{k_{-1}}C_{H_2O}\right]+\left[\frac{k_B}{k_{-1}}C_B\right]+\left[\frac{k_C}{k_{-1}}C_C\right]}}$

rate with a volumetric fraction of CO_2 ranging from 20 to 80% was supplied in the shell side of the contactor. Usually, around 15 min were necessary to reach steady-state conditions and the absorption rate was measured based on the inlet gas flow rate and the difference between the inlet and the outlet CO_2 composition in the gas.

Results and Discussion

Model validation

Examination of Figures 2 and 3 provides the ability to compare the model predictions to experimental absorption data obtained at different liquid flow rates, CO_2 partial pressures in the gas phase, and MEA concentrations in the liquid phase. The agreement between predictions and measurements is very good: the average relative deviations between calculated and experimental data are, respectively, 2.6% and 2.2% for all tests involving countercurrent and cocurrent flow. The model is able to describe very well the experimental data obtained in membrane reactors with a void fraction within the range 50–98%. Under the operation conditions of this study, the estimated PTFE membrane pore wetted fraction is bounded within the range [0–0.03]. The CO_2 absorption rate increases with the increase of the liquid flow rate, CO_2 gas concentration and MEA liquid-phase concentration and an insignificant difference between the absorption rates obtained for cocurrent and countercurrent flow can be observed.

Nonisothermal simulations

This section briefly discusses some simulation results for the nonisothermal case. The operating conditions and geometry of the hollow-fiber membrane module are listed in Table 5. The simulations are shown for the cases where the membrane pores are totally/partially filled with the gas phase. Figure 4 show the axial temperature profiles in liquid and gas phases and radial temperature profiles in the liquid film surrounding the inside membrane wall. The hollow-fiber membrane module temperature raise, which is barely perceptible, is higher for CO_2 absorption in MEA because of the highest reaction kinetics and reaction enthalpy. Figure 5 shows the influence of membrane wetting fraction on the axial temperature profiles in the liquid phase and radial temperature profiles in the liquid film surrounding the inside membrane wall and membrane liquid-filled pores. Partial wetting of membrane pores causes a significant increase of the mass transfer resistance in the membrane which decreases significantly CO_2 absorption rate and consequently the absorption module temperature.

The absorption rate is only slightly influenced by the gas-phase velocity because of the minor mass transfer resistance in the gas phase and as result, the raise of the temperature in the hollow-fiber membrane module is insignificant: for a superficial gas velocity of 0.5 m/s, comparable to the superficial velocities that are usually achieved in packed columns, the raise of the temperature for CO_2 absorption in MEA is 0.75 K. The temperature amplification increases with the increase of membrane contactor length. However, for a contactor length of 1 m, which assures a reasonable pressure drop level (30 mbar on the liquid side), and for a superficial gas velocity of 0.5 m/s (both within the industrially relevant range), the increase of the temperature in the hollow-fiber membrane module remains trivial: 1.4 K for CO_2 absorption in MEA. CO_2 absorption flux increases with the increase of inlet CO_2 partial pressure due to the higher driving force in the gas phase. As result, the temperature in the hollow-fiber membrane module increases. However, with a contactor length of 1 m, a superficial gas velocity of 0.5 m/s, and an inlet gas CO_2 mole fraction of 0.4 the increase of the temperature in the hollow-fiber membrane module remains minor: 1.6 K for CO_2 absorption in MEA.

The nonisothermal simulations reveal that the hollow-fiber membrane module operation can be considered as quasi-isothermal. This provides *post facto* justification of considering the hollow-fiber membrane module as being isothermal.

Isothermal simulations

First, simulations under membrane gas-filled pores (ideal) conditions were carried out to explore the effect of single and mixed amines solution type, liquid and gas velocity, CO_2 partial pressure, and flow orientation (cocurrent and countercurrent) on the membrane module performance. CO_2 removal by single primary (MEA), secondary (DEA), tertiary (MDEA), SHA (AMP, AMPD, AEPD, AHPD), and mixed amines (MEA-MDEA, MEA-AMP, AHPD-PZ) was studied.

Table 4. Experimental Membrane and Module Specifications

Membrane	
Material	PTFE
Inside diameter	1830 μm
Outside diameter	2440 μm
Pore diameter	0.03–0.08 μm
Porosity	0.2
Lenght	0.178 m
Module	
Number of membranes per module	8
Inside diameter	0.05 m
Length	0.178 m
Inside specific area	20.05 m^2/m^3
Outside specific area	26.73 m^2/m^3

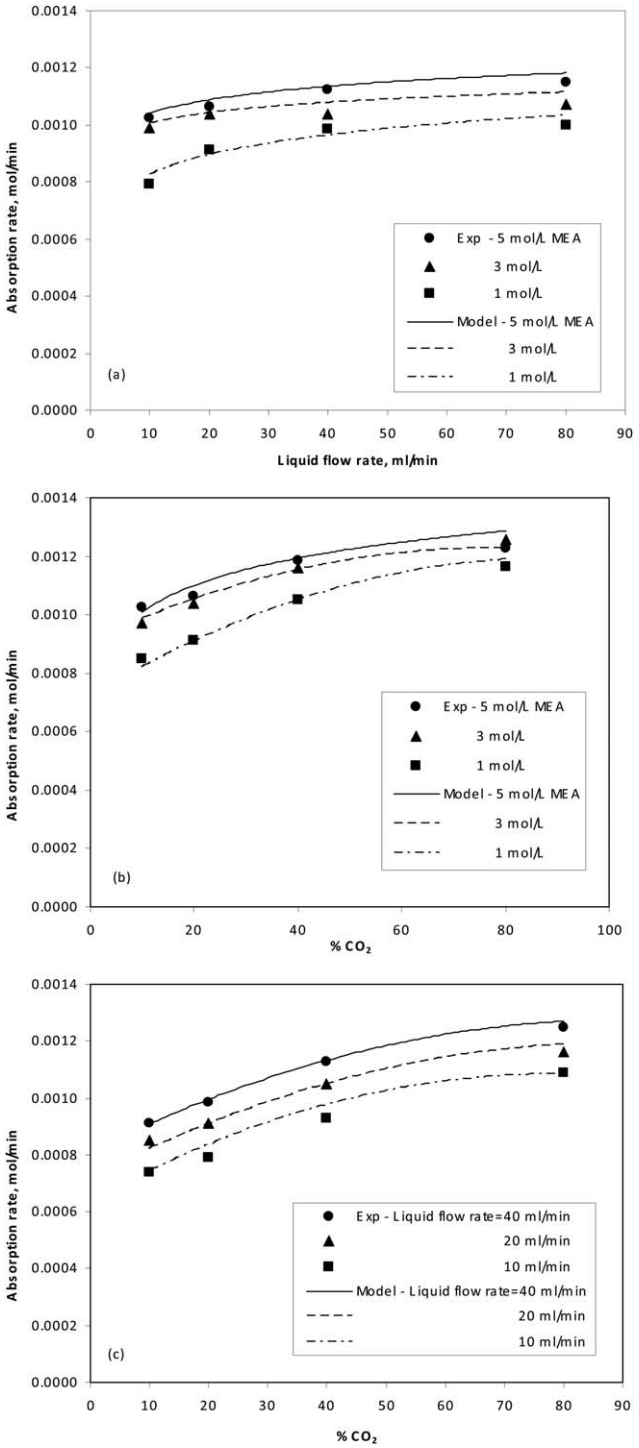

Figure 2. Experimental and theoretical CO_2 absorption rate as a function of liquid flow rate (a) and CO_2 gas concentration (b, c): gas concentration = 20% CO_2 (a); liquid flow rate = 20 ml/min (b); MEA concentration = 1 mol/L (c); gas flow rate = 300 ml/min; countercurrent flow.

Then, the influence of membrane wetting on membrane module performance was analyzed. The hollow-fiber membrane module characteristics and operating conditions used in simulation for the base case are given in Table 5.

CO_2 Absorption in Single Amine Solutions. CO_2 absorption performance of different single amines under membrane gas-filled pores conditions was analyzed. From the results

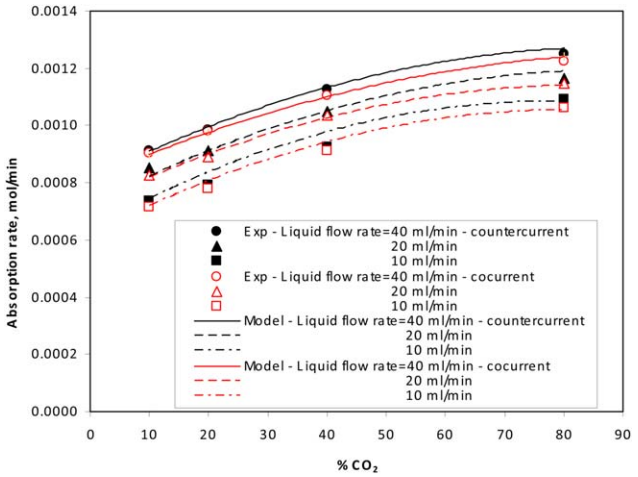

Figure 3. Predicted vs. experimental CO_2 absorption rate in the countercurrent and cocurrent HFMC: gas flow rate = 300 ml/min; MEA concentration = 1 mol/L.

[Color figure can be viewed in the online issue, which is available at wileyonlinelibrary.com.]

presented in Figure 6, it is evident that there is a strong decrease of the CO_2 absorption flux along the length of membrane for MEA and AMP because of very fast reaction of CO_2 and amine. This is coherent with the evolution of CO_2 partial pressure in the gas phase. The sharpness of the decreasing trend gradually declines for the CO_2-amine systems having lower reaction rates. There is no significant variation of the flux for the case of CO_2 absorption in MDEA due to the lower reaction rate compared to other CO_2-amine systems. MEA has the highest CO_2 absorption flux followed by AMP, AMPD, AHPD, and MDEA, which is justified from the reaction kinetics reported in Table 1. For the faster reactions (CO_2-MEA) and (CO_2-AMP) the enhancement factor defined as the ratio of absorption flux in presence of chemical reaction to the absorption flux in absence of chemical reaction increases along the length of HFMC. For the

Table 5. Hollow-Fiber Membrane Module Used in Simulations: Base Case Operating Conditions

Operating Conditions	Data
Fiber outer diameter	0.002 m
Fiber inside diameter	0.001 m
Membrane wall thickness	5×10^{-4} m
Fiber height	0.4 m
Membrane porosity	0.5
Number of fibers per module	57
Outside specific area	581.6 m^2/m^3
Inside specific area	290.8 m^2/m^3
Module void fraction	0.709
Fiber volume fraction	0.388
Reactor pressure	0.1 Mpa
Temperature	298 K
Superficial gas velocity (interstitial velocity)	0.05 m/s (0.082 m/s)
Superficial liquid velocity (interstitial velocity)	0.01 m/s (0.103 m/s)
Inlet liquid amine concentration	1 mol/L
Inlet gas CO_2 mole fraction	0.2
Module liquid fraction	0.097
Module gas fraction	0.612
Liquid-side pressure drop	0.013 bar
Gas-side pressure drop	0.055 mbar

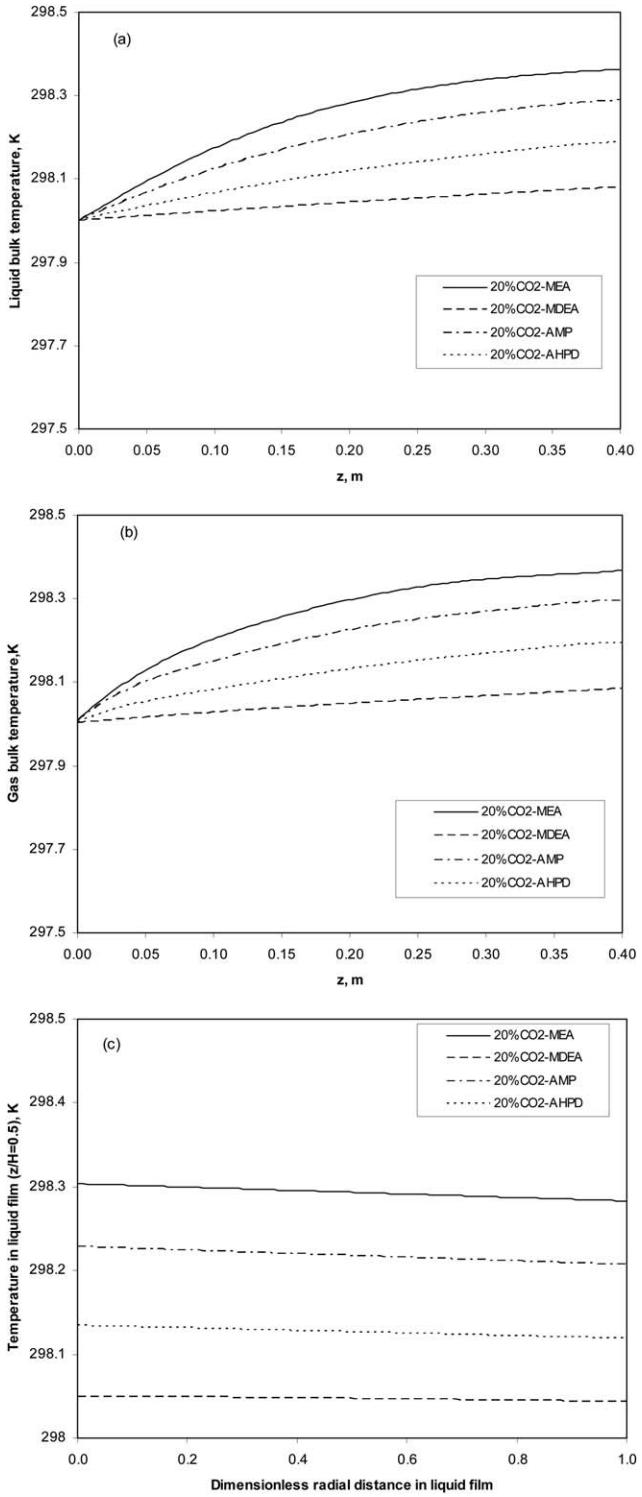

Figure 4. Axial temperature profiles (a, b) and radial temperature profiles in the liquid film (c) for CO_2 absorption in single amine solutions (base case operating conditions, nonwetted membrane, and cocurrent flow).

slowest reaction rate used in simulations (CO_2-MDEA), the enhancement factor is equal to Hatta number (not shown) and the reaction is pseudo first order. Figure 7 shows typical concentration profiles of CO_2 and amines in liquid film (the thickness of the liquid film varies between 1.025×10^{-4} and 1.22×10^{-4} m). The concentration profiles of CO_2 move to the left side of the liquid film with the increase of the reaction rate. Depletion of MEA in the liquid film is the highest due to the highest reaction rate of MEA with CO_2. MDEA is not depleted significantly and the reaction can be considered to be pseudo first order. Figure 7a shows that the

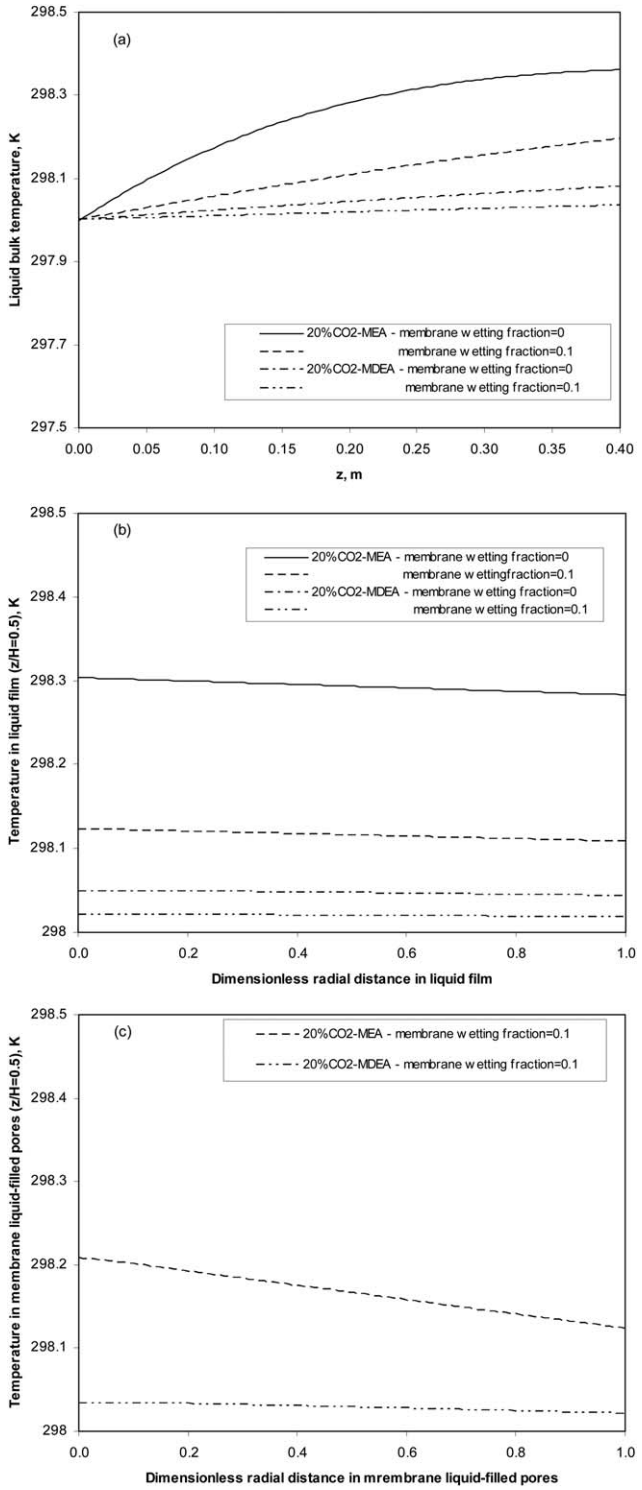

Figure 5. Influence of membrane wetting fraction on the axial temperature profiles in the liquid phase (a), radial temperature profiles in the liquid film surrounding the inside membrane wall (b), and membrane liquid-filled pores (c) (base case operating conditions, cocurrent flow).

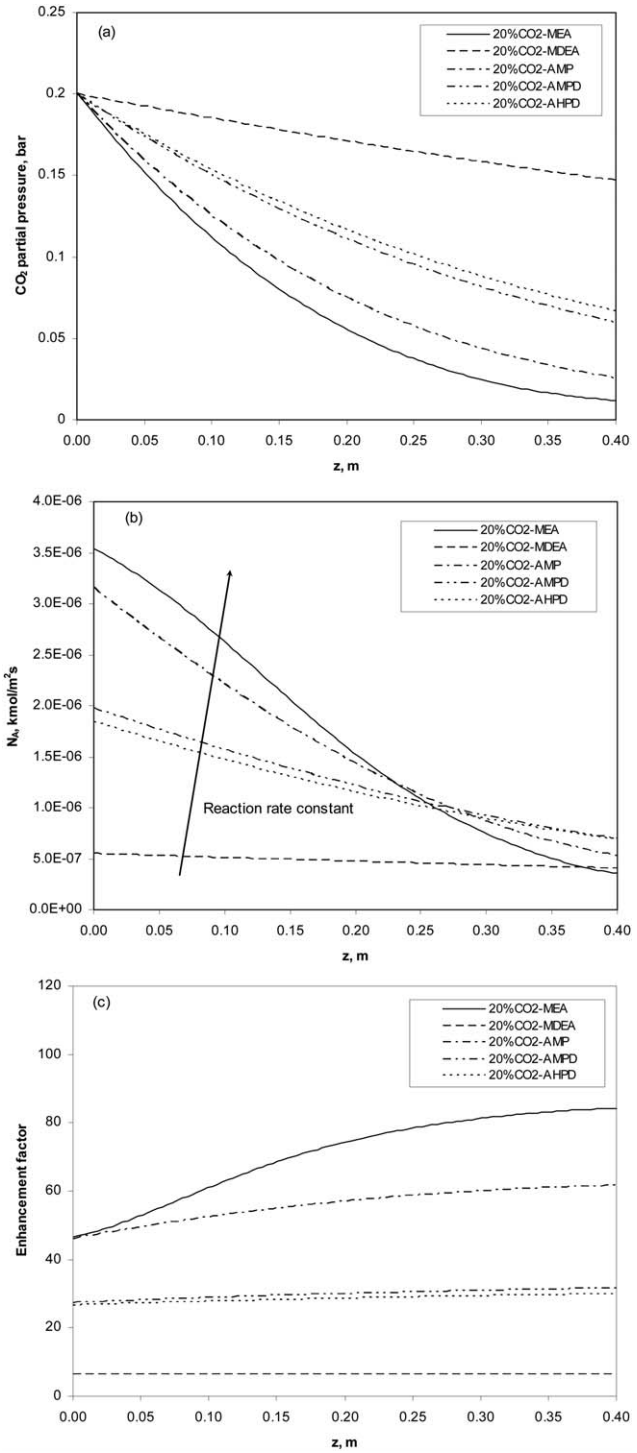

Figure 6. Axial CO_2 partial pressure (a), CO_2 absorption flux (b), and enhancement factor (c) profiles for CO_2 absorption in single amine solutions (base case operating conditions, nonwetted membrane, cocurrent flow, inlet liquid amine concentration = 1 mol/L, inlet CO_2 partial pressure = 20 vol%).

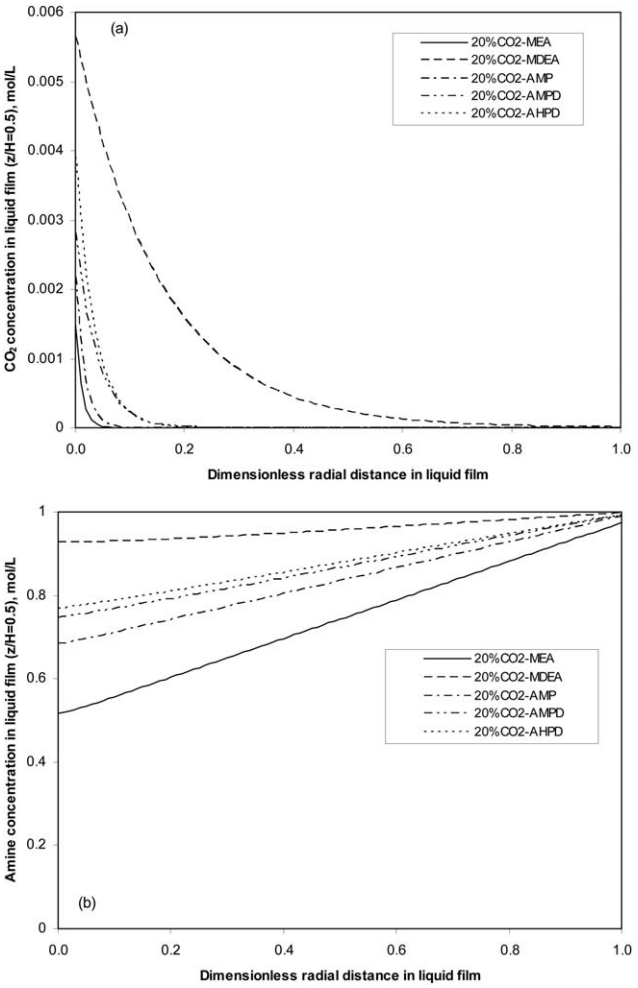

Figure 7. Liquid film CO_2 (a) and amine (b) concentration profile for CO_2 absorption in single amine solutions (base case operating conditions, nonwetted membrane, cocurrent flow, inlet liquid amine concentration = 1 mol/L, inlet CO_2 partial pressure =20 vol%).

reaction zone is confined near the inside membrane wall and consequently the liquid far from the interface is essentially undisturbed so that the depletion of amine as well as the saturation of the bulk liquid with CO_2 can be neglected. As result, "concentration plug flow" can be considered in bulk liquid, and the assumption formulated in gas–liquid membrane contactor scale model is verified.

CO_2 Absorption in Blended Amine Solutions. CO_2 absorption performance under membrane gas-filled pores conditions into aqueous blends of (MEA + MDEA), (AMP + MEA), and (AHPD + PZ) was analyzed. For CO_2 absorption in aqueous blends of (MEA + MDEA) and (AHPD + PZ) the performance of hollow-fiber membrane module (Figure 8) increases significantly with the increase of MEA and PZ concentration due to the much higher reaction rate of MEA and PZ with CO_2 (Table 2). On the other side, for CO_2 absorption in aqueous blends of (AMP + MEA) the performance of hollow-fiber membrane module is not amplified significantly by the increase of MEA concentration because the reaction rates of CO_2 with AMP and MEA are closed. The significant amplification of the performance of CO_2 absorption in the hollow-fiber membrane module when MEA and PZ concentration in aqueous blends of (MEA + MDEA) and (AHPD + PZ) increases is the results of the strong increase of the CO_2 absorption flux in the first part of the hollow-fiber membrane module (Figure 9). Figure 10 shows typical concentration profiles of CO_2 in the liquid

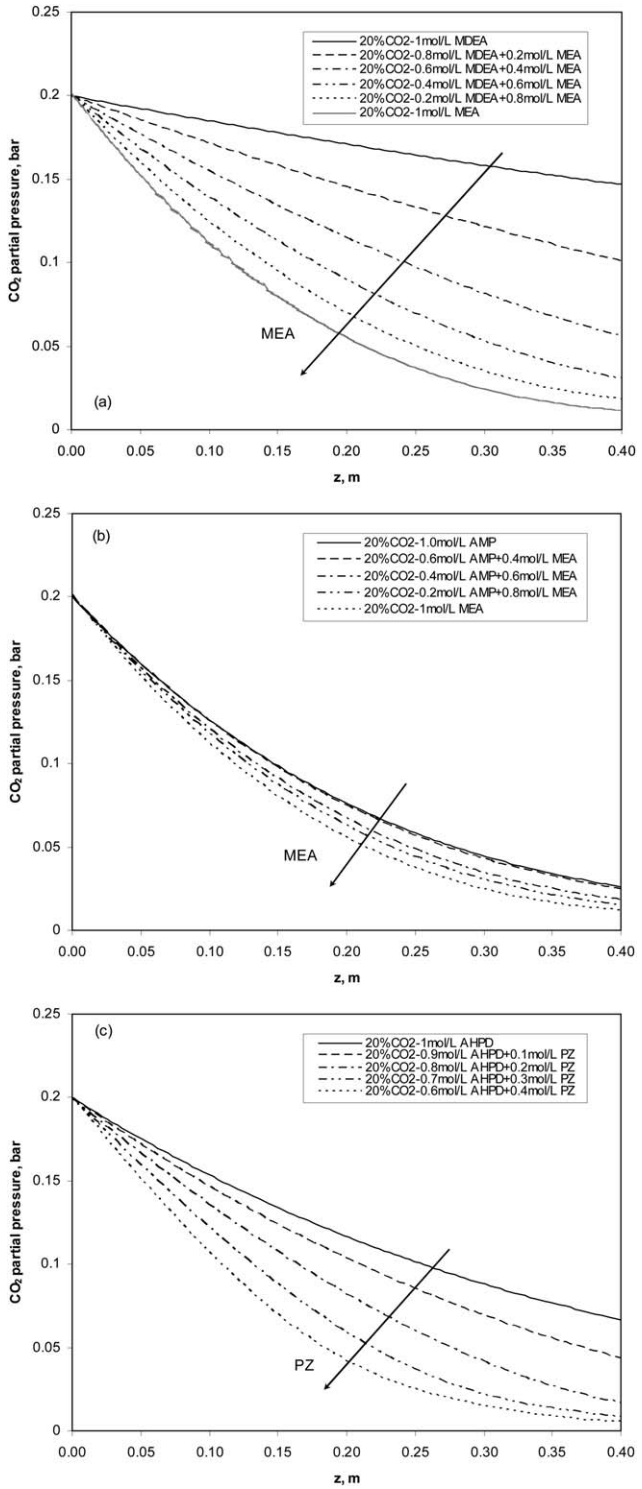

Figure 8. Axial CO_2 partial pressure profiles for CO_2 absorption in mixed amines solutions (base case operating conditions, nonwetted membrane, and cocurrent flow).

film, for CO_2 absorption in aqueous blends of (MEA + MDEA) and (AHPD + PZ). The concentration profiles of CO_2 shift to the left side of the liquid film as the concentration of MEA or Pz in amines mixture increases. The difference gradually decreases with the increase of MEA or PZ concentration because of the higher reaction rate of MEA and PZ. Similar behavior (not shown here) was obtained for the blend (AMP + MEA) but with nearer carbon dioxide concentration profiles because the reaction rates of CO_2 with AMP and MEA are closed.

Effect of Operating Conditions on CO_2 Absorption in Single Amine Solutions. Partial pressure of CO_2 in outlet gas decreases with the increase of the liquid flow rate (Figure 11a). With the increase of the liquid flow rate the thickness of the liquid boundary layer decreases and as result the mass

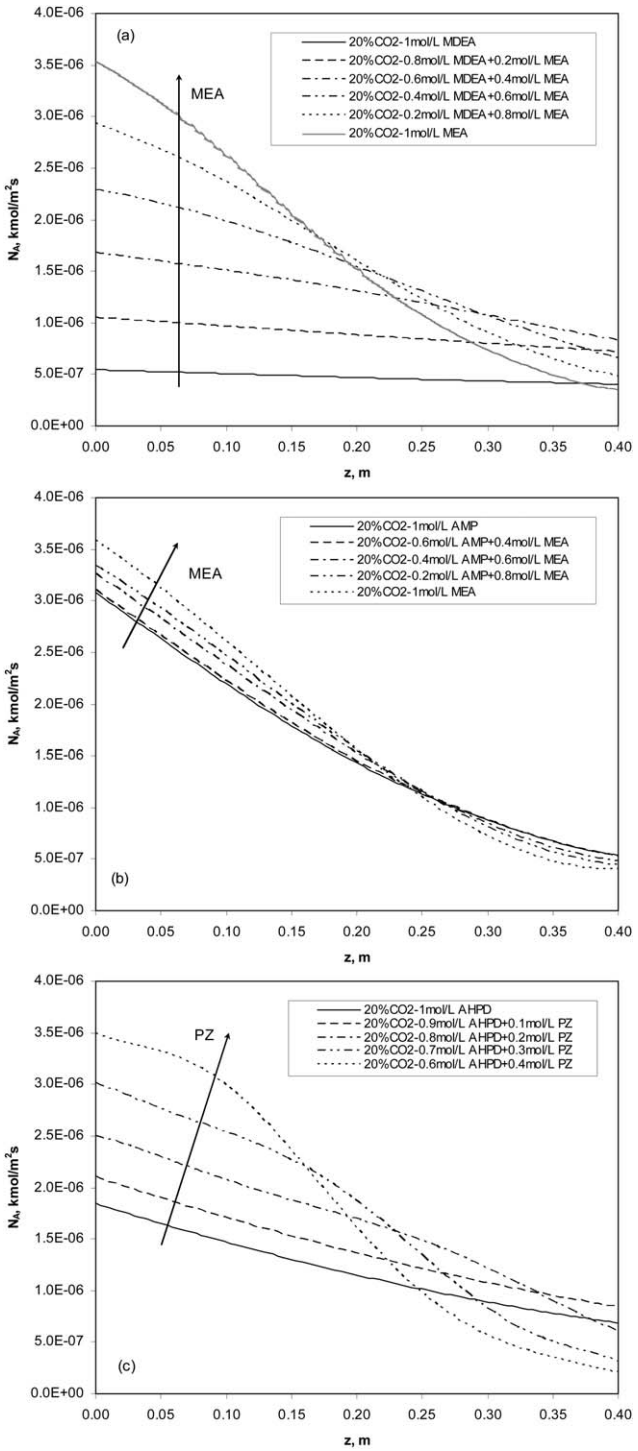

Figure 9. Axial CO_2 absorption flux profiles for CO_2 absorption in mixed amines solutions (base case operating conditions, nonwetted membrane, and cocurrent flow).

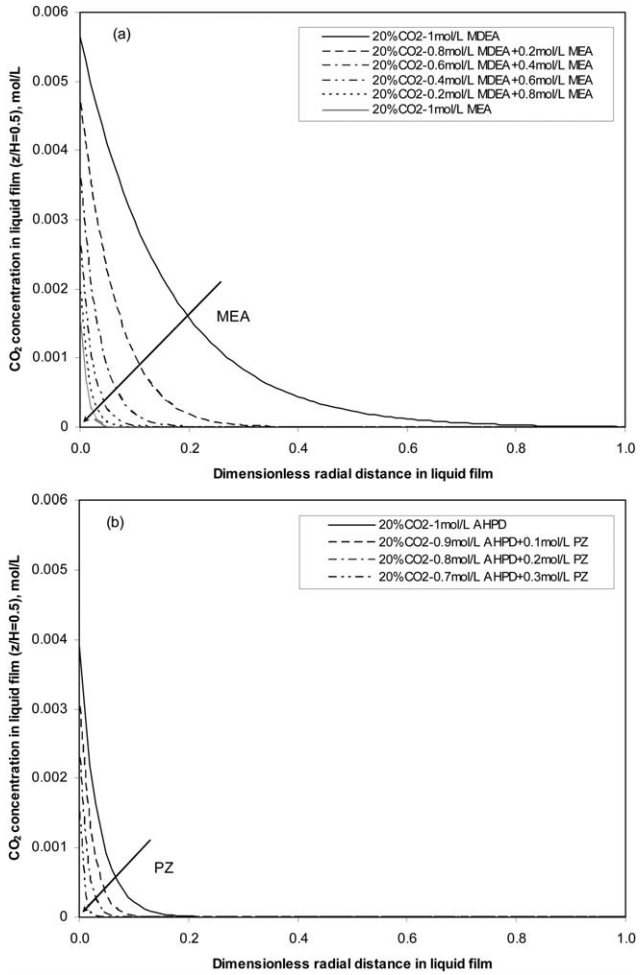

Figure 10. Liquid film CO_2 concentration profiles for CO_2 absorption in mixed amines solutions (base case operating conditions, nonwetted membrane, and cocurrent flow).

transfer resistance of the liquid side decreases and the mass transfer becomes more efficient (Figure 11b). CO_2 absorption flux increases significantly with the increase of liquid velocity in the first part of the hollow-fiber membrane module due to the intensified mass transfer and decreases slowly in the second part of hollow-fiber membrane module due to the depletion of MEA (Figure 11c). The increase of the gas flow rate causes the decrease of the gas–liquid contact time which induces a higher partial pressure of CO_2 in the gas outlet (Figure 12a). Enhancement factor and overall mass transfer coefficient (not shown) are insignificantly influenced by the gas flow rate and as result CO_2 absorption flux axial profiles follow CO_2 partial pressure profiles (Figure 12b). Therefore, the absorption rate is only slightly influenced by the gas-phase velocity, which could be attributed to a minor mass transfer resistance in the gas phase. CO_2 absorption flux increases with the increase of inlet CO_2 partial pressure (Figure 13) all along the length of the hollow-fiber membrane module due to the higher driving force in the gas phase.

Effect of Flow Orientation on the Membrane Module Performance. The simulation results of CO_2 absorption from a CO_2-N_2 (20/80 vol%) mixture flowing co- and countercurrently with DEA and AHPD solutions are presented in Figure 14. In agreement with Figure 3, an insignificant difference between the absorption in co- and countercurrent flow can be observed (CO_2 conversion in the gas phase is higher for countercurrent flow with 1.5–2%). The small difference in favor of countercurrent mode of operation is due to higher CO_2 absorption flux in the gas inlet region of hollow-fiber membrane module because countercurrent flow

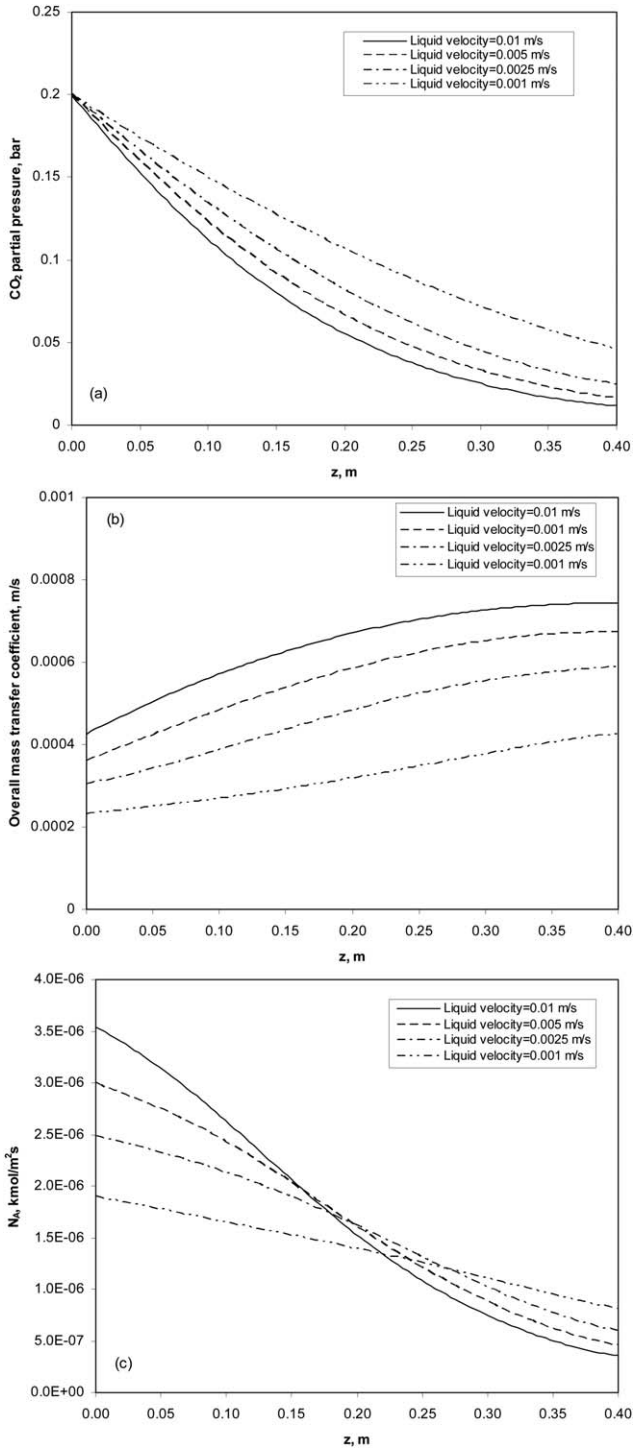

Figure 11. Axial CO_2 partial pressure (a), overall mass transfer coefficient (b), and CO_2 absorption flux (c) profiles at different liquid flow rates (20%CO_2-1 mol/L MEA system, base case operating conditions, nonwetted membrane, cocurrent flow).

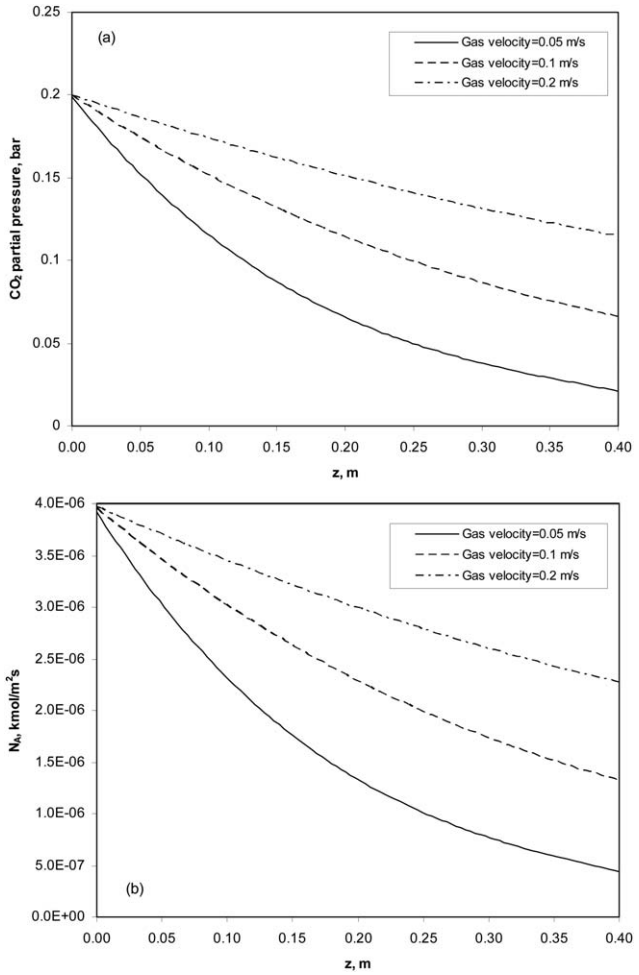

Figure 12. Axial CO_2 partial pressure (a) and CO_2 absorption flux (b) profiles at different gas flow rates (20%CO_2-1 mol/L DEA system, base case operating conditions, nonwetted membrane, cocurrent flow).

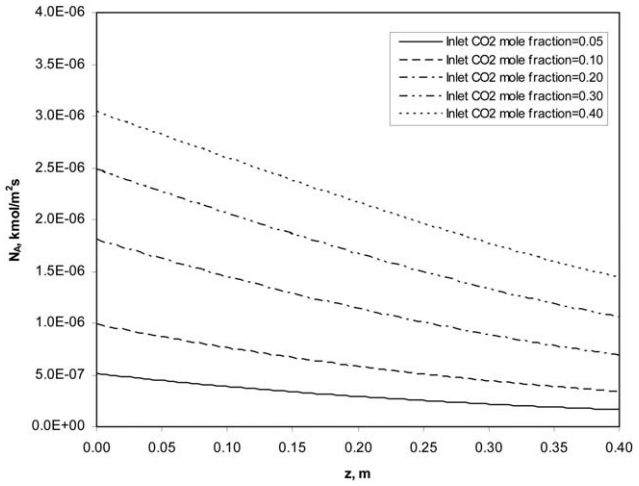

Figure 13. CO_2 absorption flux axial profiles at different values of inlet CO_2 partial pressure (1 mol/L AEPD system, base case operating conditions, nonwetted membrane, cocurrent flow).

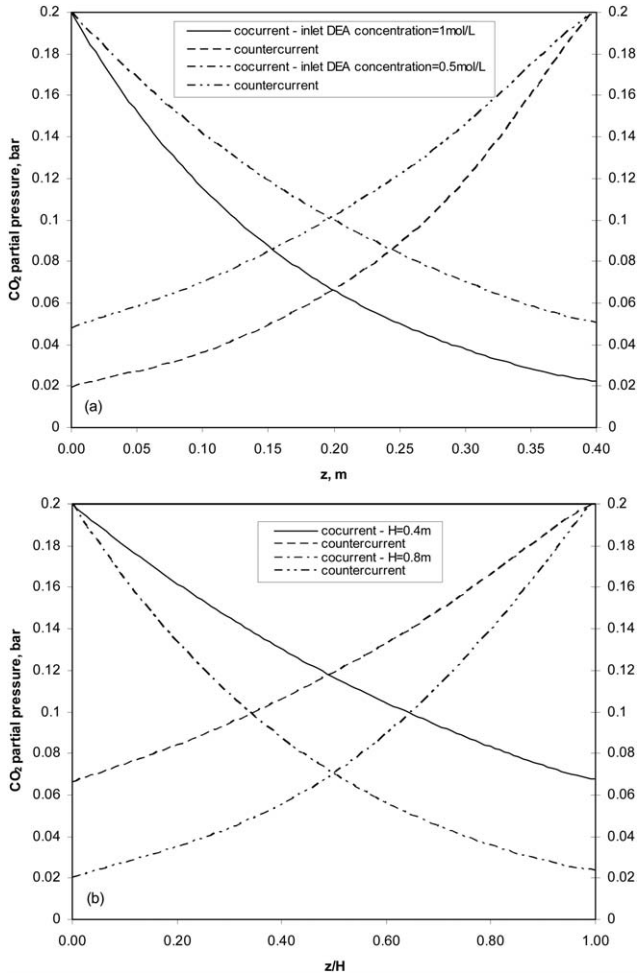

Figure 14. Axial CO_2 partial pressure profiles for co and countercurrent flow of gas and liquid phases: (a) 20%CO_2 system, (b) 20%CO_2-1 mol/L AHPD system (base case operating conditions, nonwetted membrane).

provides a higher driving force in this region. This is in agreement with the experimental results obtained in this work and the results of Kreulen et al.[30] and Atchariyawut et al.[86] obtained for the CO_2-NaOH and CO_2-MEA systems.

Effect of Membrane Wetting on the Membrane Module Performance. Partial wetting of membrane pores causes a significant increase of the mass transfer resistance in the membrane, even if the fraction of wetted pores is small, which would affect operation stability and the long-term running of the membrane contactor.[86] Figure 15 shows an important influence of the membrane wetting fraction on the performance of hollow-fiber membrane module. The increase of membrane wetting fraction decreases significantly CO_2 absorption flux especially in the first part of the hollow-fiber membrane module. This is the result of the considerably reduction of the overall mass transfer coefficient due to the amplification of the mass transfer resistance in membrane liquid-filled pores. The rate of CO_2 absorption flux reduction is more important at low wetting fractions (Figure 16), especially for AMPD, AHPD, and DEA. However, a very fast reduction of CO_2 absorption flux at small wetting fractions causes a lower CO_2 sequestration from the gas phase. As

result, the concentration of CO_2 in the gas phase increases, which increase the overall driving force of the system and slows down the future reduction of CO_2 absorption flux in time. The analysis of radial CO_2 and amines concentration distribution in liquid-filled membrane shows that the major-

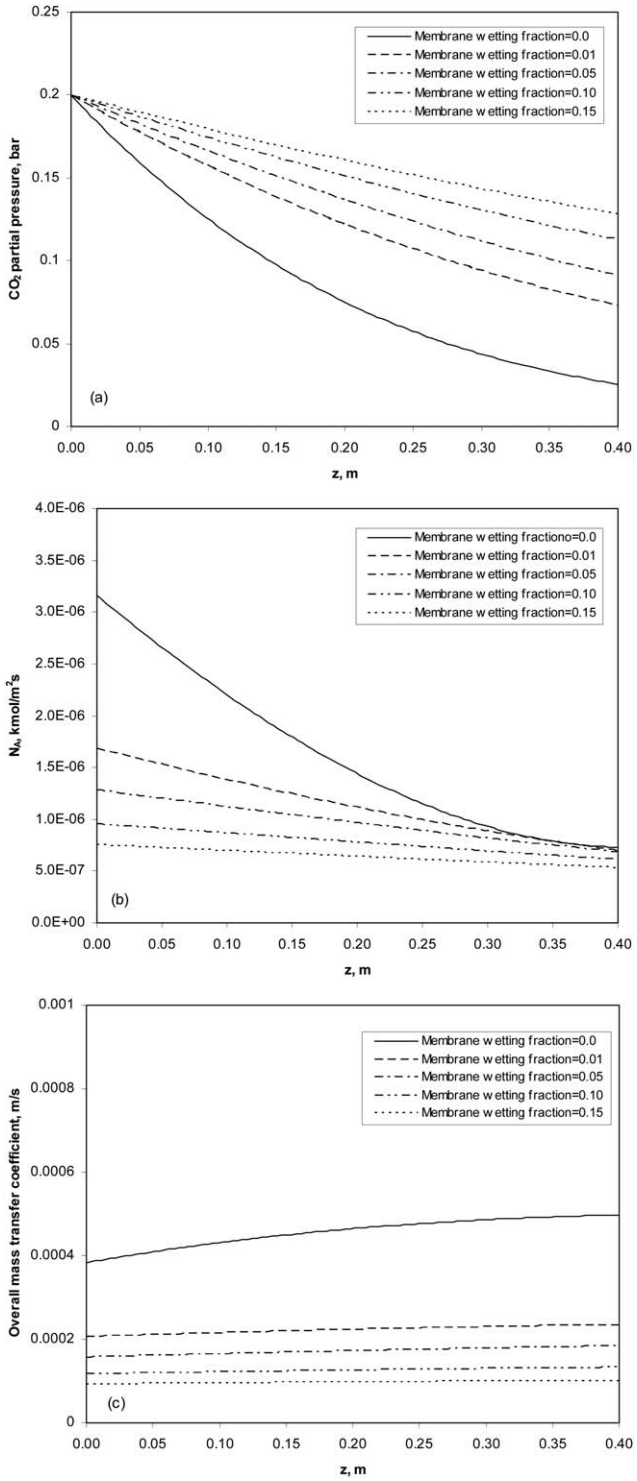

Figure 15. Axial CO_2 partial pressure (a), CO_2 absorption flux (b), and overall mass transfer coefficient (c) profiles at different values of membrane wetting fraction (20%CO_2-1 mol/L AMP system, base case operating conditions, cocurrent flow).

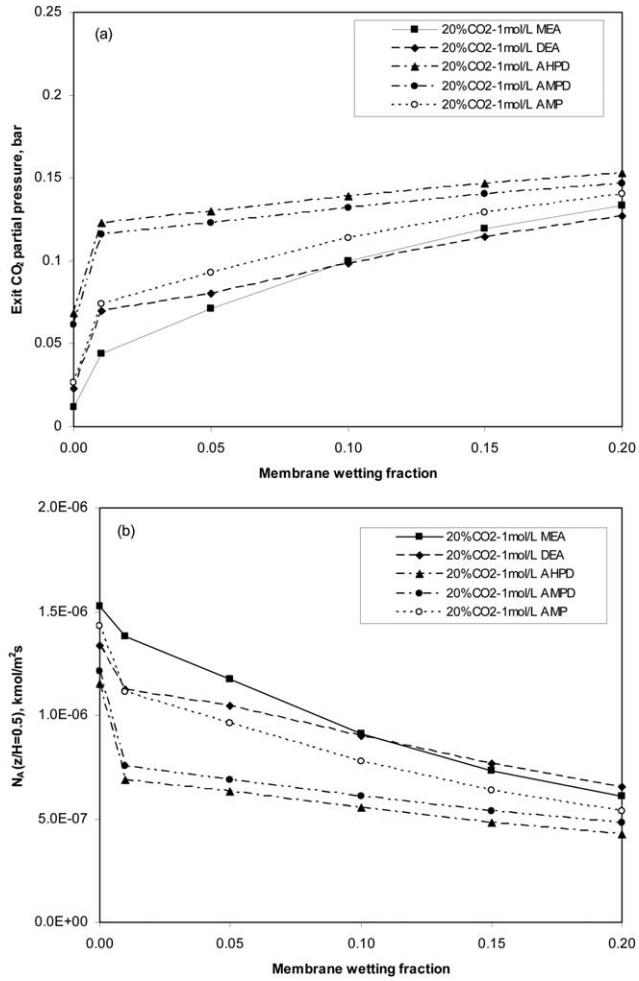

Figure 16. Exit CO_2 partial pressure (a) and CO_2 absorption flux (b) as a function of membrane wetting fraction (base case operating conditions, cocurrent flow).

ity variation of CO_2 concentration is located near the gas–liquid interface, while the amine concentration distribution is very wide in radial direction (not shown). The simulation results are in qualitatively agreement with the experimental results of Lu et al.[87]

Conclusion

CO_2 removal by single and mixed aqueous amines in HFMCs under gas-filled pores and partially liquid-filled pores conditions was studied. A two-scale, nonisothermal, steady-state model accounting for CO_2 diffusion in the gas-filled membrane pores, CO_2 and amines diffusion/reaction within the liquid-filled membrane pores, and CO_2 and amines diffusion/reaction in the liquid boundary layer was developed to simulate the comportment of a gas–liquid membrane contactor. Because the two-scale model was successful to predict the comportment of the HFMC, a series of simulations were performed to capture the effect of single and mixed amine solution type, liquid and gas velocity, inlet CO_2 partial pressure, and membrane wetting on the membrane module performance. Also, the impact of the cocurrent and countercurrent flow orientation was investigated. The conclusions can be summarized as follows: (1) MEA is the most suitable single amine solution for CO_2 absorption;

similar absorption performance was found for AHPD-Pz blend, even at low PZ concentrations; (2) there is an improvement of hollow-fiber membrane module performance with the increase of MEA or PZ concentration in aqueous blends of (MEA + MDEA), (AMP + MEA), and (AHPD + PZ); (3) for both membrane gas-filled and partially liquid-filled pores conditions the reaction zone is located near the gas–liquid interface which is positioned at the membrane wall, respectively, inside the membrane; (4) membrane wetting, even at low fractions, decreases significantly the performance of hollow-fiber membrane module; (5) an insignificant difference between the absorption in cocurrent and countercurrent flow was observed in this study; (6) nonisothermal simulations reveal that the hollow-fiber membrane module operation can be considered as quasi-isothermal.

Notation

a_v^{in} = inside specific area, m^2/m^3
a_v^{out} = outside specific area, m^2/m^3
$c_{p,\alpha}$ = specific heat capacity of α-phase (α=g, l), J/kgK
C_j = concentration of species j, kmol/m^3
d_m^{in} = inner diameter of hollow-fiber membrane, m
d_m^{out} = outer diameter of hollow-fiber membrane, m
$D_{j,\alpha}$ = molecular diffusivity coefficient of species j in α phase (α=g, l), m^2/s
$D_{j,\alpha}^{eff}$ = effective diffusivity of species j inside membrane (α=g, l), m^2/s
D_{kj} = Knudsen diffusion coefficient of species j, m^2/s
H = membrane length, m
k_g = gas-phase mass transfer coefficient, m/s
k_l = liquid-phase mass transfer coefficient, m/s
m = distribution coefficient
N_A = mass transfer flux of solute A, $N_A = -D_{j,A}^{eff}\frac{\partial C^l_{A,m}}{\partial r}|_{r=R_m^{in}} = -D_{A,l}\frac{\partial C_{A,lf}}{\partial r}|_{r=R_m^{in}}$
Nu = Nusselt number
P = pressure, bar
Pr = Prandtl number
r = radial position within porous membrane and liquid film, m
r_i = reaction rate of reaction i, kmol/m^3s
r_{CO_2-j} = reaction rate, kmol/m^3s
r_m^{out} = outer hollow-fiber membrane radius, m
R = ideal-gas constant
R_j = reaction rate of the component j, kmol/m^3s
R^{lf} = radius of liquid film surrounding the hollow-fiber membrane, m
R_m^{gl} = radius of gas–liquid interface in hollow-fiber membrane, m
R_m^{in} = inner radius of hollow-fiber membrane, m
R_m^{out} = outer radius of hollow-fiber membrane, m
Re = Reynolds number
Sc = Schmidt number
Sh = Sherwood number
T = temperature, K
u_g = superficial gas velocity, m/s
u_ℓ = superficial liquid velocity, m/s
z = axial coordinate, m

Greek letters

α_g = gas-phase heat transfer coefficient, kJ/m^2sK
δ = membrane wall thickness, m
ΔH_r = reaction enthalpy, KJ/Kmol
ε = membrane porosity
ε_α = module α-phase fraction
φ = fiber volume fraction
κ = Kozeny constant
λ_α = conductivity of α-phase, kJ/msK
μ_α = dynamic viscosity of α-phase, kg/m s
$v_{A,i}$ = stoichiometric coefficient of CO_2 in reaction i
τ = tortuosity factor

Subscripts/superscripts

g = gas phase
in = inlet, inside
l = liquid phase
lf = liquid film
m = membrane
s = solid phase
out = outer, outside

Abbreviations

Am = amine in the system, MDEA or Pz

Literature Cited

1. IPCC. *Climate Change 2014: Mitigation of Climate Change, vol.Intergovernmental Panel on Climate Change. Working Group III*. Cambridge: Cambridge University Press, for the Intergovernmental Panel on Climate Change, 2014.
2. Aaron D, Tsouris C. Separation of CO_2 from flue gas: a review. *Sep. Sci. Technol*. 2005;40:321–348.
3. Stewart C, Hessami MA. A study of methods of carbon dioxide capture and sequestration—the sustainability of a photosynthetic bioreactor approach. *Energy Convers Manag*. 2005;46:403–420.
4. Figueroa JD, Fout T, Plasynski S, McIlvried H, Srivastava RD. Advances in CO_2 capture technology—The US Department of Energy's Carbon Sequestration Program. *Int. J. Greenhouse Gas Control*. 2008;2:9–20.
5. Luis P, Van Gerven T, Van der Bruggen B. Recent developments in membrane-based technologies for CO_2 capture. *Prog. Energy Combust. Sci*. 2012;38:419–448.
6. Kohl AL, Nielsen R. *Gas Purification*, *5th ed*. Houston, TX: Gulf Publishing Company, 1997.
7. Penders-van Elk N, Derks PWJ, Fradette S, Versteeg GF. Kinetics of absorption of carbon dioxide in aqueous MDEA solutions with carbonic anhydrase at 298 K. *Int. J. Greenhouse Gas Control*. 2012; 9:385–392.
8. Jackson P, Attalla M. Environmental impacts of post-combustion capture—new insights. In: *10th International Conference on Greenhouse Gas Control Technologies, vol. 4*. 2011:2277–2284.
9. Idem R, Wilson M, Tontiwachwuthikul P, Chakma A, Veawab A, Aroonwilas A, Gelowitz D. Pilot plant studies of the CO_2 capture performance of aqueous MEA and mixed MEA/MDEA solvents at the University of Regina CO_2 capture technology development plant and the Boundary Dam CO_2 capture demonstration. *Ind. Eng. Chem. Res*. 2006;45:2414–2420.
10. Barzagli F, Mani F, Peruzzini M. Continuous cycles of CO_2 absorption and amine regeneration with aqueous alkanolamines: a comparison of the efficiency between pure and blended DEA, MDEA and AMP solutions by C^{13} NMR spectroscopy. *Energy Environ. Sci*. 2010;3:772–779.
11. Bishnoi S, Rochelle GT. Absorption of carbon dioxide into aqueous piperazine: reaction kinetics, mass transfer and solubility. *Chem. Eng. Sci*. 2000;55:5531–5543.
12. Soosaiprakasam IR, Veawab A. Corrosion and polarization behavior of carbon steel in MEA-based CO_2 capture process. *Int. J. Greenhouse Gas Control*. 2008;2:553–562.
13. Saiwan C, Supap T, Idem RO, Tontiwachwuthikul P. Part 3: corrosion and prevention in post-combustion CO_2 capture systems. *Carbon Manag*. 2011;2:659–675.
14. Strazisar BR, Anderson RR, White CM. Degradation pathways for monoethanolamine in a CO_2 capture facility. *Energy Fuels* 2003;17: 1034–1039.
15. Bougie F, Iliuta MC. Stability of aqueous amine solutions to thermal and oxidative degradation in the absence and the presence of CO_2. *Int. J. Greenhouse Gas Control*. 2014;29:16–21.
16. Xu GW, Zhang CF, Qin SJ, Wang YW. Kinetics study on absorption of carbon dioxide into solutions of activated methyldiethanolamine. *Ind. Eng. Chem. Res*. 1992;31:921–927.
17. Zhang X, Zhang CF, Qin SJ, Zheng ZS. A kinetics study on the absorption of carbon dioxide into a mixed aqueous solution of methyldiethanolamine and piperazine. *Ind. Eng. Chem. Res*. 2001;40:3785–3791.
18. Seo DJ, Hong WH. Effect of piperazine on the kinetics of carbon dioxide with aqueous solutions of 2-amino-2-methyl-1-propanol. *Ind. Eng. Chem. Res*. 2000;39:2062–2067.
19. Yeon SH, Sea B, Park YI, Lee KS, Lee KH. Absorption of carbon dioxide characterized using the absorbent composed of piperazine and triethanolamine. *Sep. Sci. Technol*. 2004;39:3281–3300.
20. Bougie F, Lauzon-Gauthier J, Iliuta MC. Acceleration of the reaction of carbon dioxide into aqueous 2-amino-2-hydroxymethyl-1,3-propanediol Solutions by piperazine addition. *Chem. Eng. Sci*. 2009;64:2011–2019.

21. Bougie F, Iliuta MC. Kinetics of absorption of carbon dioxide into aqueous solutions of 2-amino-2-hydroxymethyl-1,3-propanediol. *Chem. Eng. Sci.* 2009;64:153–162.
22. Falk-Pedersen O, Dannström H. Separation of carbon dioxide from offshore gas turbine exhaust. *Energy Convers. Manag.* 1997;38:S81–S86.
23. deMontigny D, Tontiwachwuthikul P, Chakma A. Comparing the absorption performance of packed columns and membrane contactors. *Ind. Eng. Chem. Res.* 2005;44:5726–5732.
24. Karoor S, Sirkar KK. Gas absorption studies in microporous hollow fiber membrane modules. *Ind. Eng. Chem. Res.* 1993;32:674–684.
25. Sirkar KK. Other new membrane processes. In: Winston Ho WS, Sirkar KK, editors. *Membrane Handbook*. New York: Van Nostrand Reinhold, 1992:885–912.
26. Mosadegh-Sedghi S, Rodrigue D, Brisson J, Iliuta MC. Wetting phenomenon in membrane contactors—causes and prevention. *J. Membr. Sci.* 2014;452:332–353.
27. Franco J, Demontigny D, Kentish S, Perera J, Stevens G. A study of the mass transfer of CO_2 through different membrane materials in the membrane gas absorption process. *Sep. Sci. Technol.* 2008;43:225–244.
28. Gabelman A, Hwang ST. Hollow fiber membrane contactors. *J. Membr. Sci.* 1999;159:61–106.
29. Dindore VY, Brilman DWF, Geuzebroek FH, Versteeg GF. Membrane-solvent selection for CO_2 removal using membrane gas-liquid contactors. *Sep. Purif. Technol.* 2004;40:133–145.
30. Kreulen H, Smolders CA, Versteeg GF, Van Swaaij WPM. Microporous hollow fibre membrane modules as gas-liquid contactors. Part 2. Mass transfer with chemical reaction. *J. Membr. Sci.* 1993;78:217–238.
31. Bhaumik S, Majumdar S, Sirkar KK. Hollow-fiber membrane-based rapid pressure swing absorption. *AIChE J.* 1996;42:409–421.
32. Wang R, Li DF, Liang DT. Modeling of CO_2 capture by three typical amine solutions in hollow fiber membrane contactors. *Chem. Eng. Process.* 2004;43:849–856.
33. Hoff KA, Juliussen O, Falk-Pedersen O, Svendsen HF. Modeling and experimental study of carbon dioxide absorption in aqueous alkanolamine solutions using a membrane contactor. *Ind. Eng. Chem. Res.* 2004;43:4908–4921.
34. Zhang HY, Wang R, Liang DT, Tay JH. Modeling and experimental study of CO_2 absorption in a hollow fiber membrane contactor. *J. Membr. Sci.* 2006;279:301–310.
35. Gong YW, Wang Z, Wang SC. Experiments and simulation of CO_2 removal by mixed amines in a hollow fiber membrane module. *Chem. Eng. Process.* 2006;45:652–660.
36. Paul S, Ghoshal AK, Mandal B. Removal of CO_2 by single and blended aqueous alkanolamine solvents in hollow-fiber membrane contactor: modeling and simulation. *Ind. Eng. Chem. Res.* 2007;46:2576–2588.
37. Delgado JA, Uguina MA, Sotelo JL, Agueda VI, Sanz A. Simulation of CO_2 absorption into aqueous DEA using a hollow fiber membrane contactor: evaluation of contactor performance. *Chem. Eng. J.* 2009;152:396–405.
38. Khaisri S, deMontigny D, Tontiwachwuthikul P, Jiraratananon R. A mathematical model for gas absorption membrane contactors that studies the effect of partially wetted membranes. *J. Membr. Sci.* 2010;347:228–239.
39. Rode S, Phuc Tien N, Roizard D, Bounaceur R, Castel C, Favre E. Evaluating the intensification potential of membrane contactors for gas absorption in a chemical solvent: a generic one-dimensional methodology and its application to CO_2 absorption in monoethanolamine. *J. Membr. Sci.* 2012;389:1–16.
40. Boucif N, Corriou JP, Roizard D, Favre E. Carbon dioxide absorption by monoethanolamine in hollow fiber membrane contactors: a parametric investigation. *AIChE J.* 2012;58:2843–2855.
41. Ghasem N, Al-Marzouqi M, Rahim NA. Modeling of CO_2 absorption in a membrane contactor considering solvent evaporation. *Sep. Purif. Technol.* 2013;110:1–10.
42. Zaidiza DA, Billaud J, Belaissaoui B, Rode S, Roizard D, Favre E. Modeling of CO_2 post-combustion capture using membrane contactors, comparison between one- and two-dimensional approaches. *J. Membr. Sci.* 2014;455:64–74.
43. Chabanon E, Roizard D, Favre E. Modeling strategies of membrane contactors for post-combustion carbon capture: a critical comparative study. *Chem. Eng. Sci.* 2013;87:393–407.
44. Lee JC, Yetter RA, Dryer FL, Tomboulides AG, Orszag SA. Simulation and analysis of laminar flow reactors. *Combust. Sci. Technol.* 2000;159:199–212.
45. Iliuta I, Iliuta MC, Larachi F. Catalytic CO_2 hydration by immobilized and free human carbonic anhydrase II in a laminar flow microreactor—model and simulations. *Sep. Purif. Technol.* 2013;107:61–69.
46. Lewis WK, Whitman WG. Principles of gas absorption. *Ind. Eng. Chem.* 1924;16:1215–1220.
47. Caplow M. Kinetics of carbamate formation and breakdown. *J. Am. Chem. Soc.* 1968;90:6795–6803.
48. Danckwerts PV. The reaction of CO_2 with ethanolamines. *Chem. Eng. Sci.* 1979;34:443–446.
49. Blauwhoff PMM, Versteeg GF, Van Swaaij WPM. A study on the reaction between CO_2 and alkanolamines in aqueous solutions. *Chem. Eng. Sci.* 1984;39:207–225.
50. Yoon SJ, Lee H, Yoon JH, Shim JG, Lee JK, Min BY, Eum HM. Kinetics of absorption of carbon dioxide into aqueous 2-amino-2-ethyl-1,3-propanediol solutions. *Ind. Eng. Chem. Res.* 2002;41:3651–3656.
51. Yoon JH, Baek JI, Yamamoto Y, Komai T, Kawamura T. Kinetics of removal of carbon dioxide by aqueous 2-amino-2-methyl-1,3-propanediol. *Chem. Eng. Sci.* 2003;58:5229–5237.
52. Sun WC, Yong CB, Li MH. Kinetics of the absorption of carbon dioxide into mixed aqueous solutions of 2-amino-2-methyl-l-propanol and piperazine. *Chem. Eng. Sci.* 2005;60:503–516.
53. Froment GF, De Wilde J, Bischoff KB. *Chemical Reactor Analysis and Design*, 3rd ed. Hoboken, NJ: Wiley, 2011.
54. Kobayashi T, Laidler KJ. Theory of kinetics of reactions catalyzed by enzymes attached to membranes. *Biotechnol. Bioeng.* 1974;16:77–97.
55. Paul S, Ghoshal AK, Mandal B. Theoretical studies on separation of CO_2 by single and blended aqueous alkanolamine solvents in flat sheet membrane contactor (FSMC). *Chem. Eng. J.* 2008;144:352–360.
56. Happel J. Viscous flow relative to arrays of cylinders. *AIChE J.* 1959;5:174–177.
57. van den Berg GB, Smolders CA. Diffusional phenomena in membrane separation process. *J. Membr. Sci.* 1992;73:103–118.
58. Reid RC, Prausnitz JM, Poling BE. *The Properties of Gases and Liquids*, *4th ed*. New York: McGraw-Hill, 1987.
59. Treybal RE. *Mass-Transfer Operations*, *2nd ed*. New York: McGraw-Hill, 1967.
60. Versteeg GF, Van Swaaij WPM. Solubility and diffusivity of acid gases (CO_2, N_2O) in aqueous alkanolamine solutions. *J. Chem. Eng. Data.* 1988;33:29–34.
61. Thomas WJ, Furzer IA. Diffusion measurements in liquids by the Gouy method. *Chem. Eng. Sci.* 1962;17:115–120.
62. Poling BE, Prausnitz JM, O'Connell JP. *The Properties of Gases and Liquids*, *5th ed*. New York: McGraw-Hill, 2001.
63. Harriott P. Thermal conductivity of catalyst pellets and other porous particles. Part I: review of models and published results. *Chem. Eng. J.* 1975;10:65–71.
64. Pagé M, Huot JY, Jolicoeur C. A comprehensive thermodynamic investigation of water ethanolamine mixtures at 10, 25, and 40°C. *Can. J. Chem.-Rev. Can. Chim.* 1993;71:1064–1072.
65. Chiu LF, Li MH. Heat capacity of alkanolamine aqueous solutions. *J. Chem. Eng. Data.* 1999;44:1396–1401.
66. Zhang Y, Chen CC. Thermodynamic modeling for CO_2 absorption in aqueous MDEA solution with electrolyte NRTL model. *Ind. Eng. Chem. Res.* 2011;50:163–175.
67. Olivia RW, Leron RB, Li MH. Molar heat capacities of aqueous 2-amino-2-ethyl-1,3-propanediol solutions and their ternary mixtures containing piperazine or lithium salts. *Fluid Phase Equilibr.* 2014;365:74–79.
68. Olivia RW, Leron RB, Li MH. Heat capacities of aqueous ternary mixtures of 2-amino-2-methyl-1, 3-propanediol + piperazine or lithium bromide. *Int. J. Chem. Eng. Appl.* 2014;5:85–89.
69. Arcis H, Rodier L, Ballerat-Busserolles K, Coxam JY. Modeling of (vapor plus liquid) equilibrium and enthalpy of solution of carbon dioxide (CO(2)) in aqueous methyldiethanolamine (MDEA) solutions. *J. Chem. Thermodyn.* 2009;41:783–789.
70. Gabrielsen J, Michelsen ML, Stenby EH, Kontogeorgis GM. Modeling of CO_2 absorber using an AMP solution. *AIChE J.* 2006;52:3443–3451.
71. Park JY, Yoon SJ, Lee H, Yoon JH, Shim JG, Lee JK, Min BY, Eum HM, Kang MC. Solubility of carbon dioxide in aqueous

solutions of 2-amino-2-ethyl-1,3-propanediol. *Fluid Phase Equilibr*. 2002;202:359–366.
72. Baek JI, Yoon JH. Solubility of carbon dioxide in aqueous solutions of 2-amino-2-methyl-1,3-propanediol. *J. Chem. Eng. Data*. 1998;43: 635–637.
73. Rodier L, Ballerat-Busserolles K, Coxam JY. Enthalpy of absorption and limit of solubility of CO_2 in aqueous solutions of 2-amino-2-hydroxymethyl-1,3-propanediol, 2-2-(dimethyl-amino)ethoxy ethanol, and 3-dimethyl-amino-1-propanol at T = (313.15 and 353.15) K and pressures up to 2 MPa. *J. Chem. Thermodyn*. 2010;42:773–780.
74. Liu JZ, Wang SJ, Svendsen HF, Idrees MU, Kim I, Chen CH. Heat of absorption of CO_2 in aqueous ammonia, piperazine solutions and their mixtures. *Int. J. Greenhouse Gas Control*. 2012;9:148–159.
75. Mathonat C, Majer V, Mather AE, Grolier JPE. Use of flow calorimetry for determining enthalpies of absorption and the solubility of CO_2 in aqueous monoethanolamine solutions. *Ind. Eng. Chem. Res*. 1998;37:4136–4141.
76. Kim I, Svendsen HF. Heat of absorption of carbon dioxide (CO_2) in monoethanolamine (MEA) and 2-(Aminoethyl)ethanolamine (AEEA) solutions. *Ind. Eng. Chem. Res*. 2007;46:5803–5809.
77. Yang MC, Cussler EL. Designing hollow-fiber contactors. *AIChE J*. 1986;32:1910–1916.
78. Feron PHM, Jansen AE. CO_2 separation with polyolefin membrane contactors and dedicated absorption liquids: performances and prospects. *Sep. Purif. Technol*. 2002;27:231–242.
79. Sparrow EM, Abraham JP, Tong JCK. Archival correlations for average heat transfer coefficients for non-circular and circular cylinders and for spheres in cross-flow. *Int. J. Heat Mass Transfer*. 2004; 47:5285–5296.
80. Liao CH, Li MH. Kinetics of absorption of carbon dioxide into aqueous solutions of monoethanolamine + *N*-methyldiethanolamine. *Chem. Eng. Sci*. 2002;57:4569–4582.
81. Xu S, Wang YW, Otto FD, Mather AE. Kinetics of the reaction of carbon dioxide with 2-amino-2-methyl-1-propanol Solutions. *Chem. Eng. Sci*. 1996;51:841–850.
82. Littel RJ, Versteeg GF, Van Swaaij WPM. Kinetics of CO_2 with primary and secondary amines in aqueous solutions—I. Zwitterion deprotonation kinetics for DEA and DIPA in aqueous blends of alkanolamines. *Chem. Eng. Sci*. 1992;47:2027–2035.
83. Ali SH. Kinetics of the reaction of carbon dioxide with blends of amines in aqueous media using the stopped-flow technique. *Int. J. Chem. Kinet*. 2005;37:391–405.
84. Kumar PS, Hogendoorn JA, Feron PHM, Versteeg GF. New absorption liquids for the removal of CO_2 from dilute gas streams using membrane contactors. *Chem. Eng. Sci*. 2002;57:1639–1651.
85. Bougie F, Iliuta I, Iliuta MC. Absorption of CO2 by AHPD-Pz aqueous blend in PTFE hollow fiber membrane contactors. *Sep. Purif. Technol*. 2014;138:84–91.
86. Atchariyawut S, Jiraratananon R, Wang R. Separation of CO_2 from CH_4 by using gas-liquid membrane contacting process. *J. Membr. Sci*. 2007;304:163–172.
87. Lu JG, Wang LJ, Sun XY, Li JS, Liu XD. Absorption of CO_2 into aqueous solutions of methyldiethanolamine and activated methyldiethanolamine from a gas mixture in a hollow fiber contactor. *Ind. Eng. Chem. Res*. 2005;44:9230–9238.

Manuscript received Aug. 22, 2014, and revision received Oct. 17, 2014.